TECHNISCHE UNIVERSITÄT WIEN
Vienna University of Technology

Diplomarbeit

Building a cryostate for Cryo Fluorescence Microscopy

zur Erlangung des akademischen Grades

Diplom-Ingeneur

im Rahmen des Studiums

Master technische Physik

eingereicht von

Lukas Sparer
Matrikelnummer 01225496

ausgeführt am Institut für Angewandte Physik
der Fakultät für Physik der Technischen Universität Wien

Betreuer: Univ.Prof. Dipl.-Ing. Dr. Gerhard Schütz
Mitwirkung: PhD Montserrat Lopez

Ort, Datum	(Unterschrift Verfasser)	(Unterschrift Betreuer)

Aknowledgements

Big thanks to TU Vienna and PhD Montserrat Lopez for the big support and knowledge that had been given to me while adapting the setup until it worked.

Contents

Aknowledgements i

List of Figures vi

1 Abstract 1

2 Introduction 1
2.1 The Fluorophore-Fluorescence . . . 1
2.2 High resolution Microscopy . . . 2
2.2.1 The Diffraction-Limited Resolution of Light Microscopy . . . 2
2.3 Single fluorescent molecule detection . . . 4
2.3.1 Confocal Microscopy . . . 4
2.3.2 Structured Illumination Microscopy (SIM) . . . 6
2.4 Super resolution microscopy . . . 6
2.4.1 Stimulated emission depletion microscopy(STED) . . . 6
2.4.2 Single molecule localization microscopy(SMLM) . . . 8
2.5 Cryo Super Resolution Microscopy (Cryo SMLM) . . . 9

3 Cryostat design 11
3.1 Coupling of cooling components . . . 13
3.2 Measurements at cryogenic temperatures . . . 17
3.3 Optical setup . . . 17
3.4 Triggering two lasers separately . . . 22
3.5 Installing the Piezo Controller . . . 24
3.6 Installing the vacuum pump . . . 24
3.7 Installing the temperature probe . . . 26
3.8 Thermal stability . . . 28

4 Experimental Methods 30
4.1 Sample preparation . . . 30
4.2 Photostability measurements . . . 30
4.3 Analysis . . . 31

5 Results and Discussion 32
5.1 Measurements at room temperature (T=293K) . . . 32
5.2 Measurements at cryogenic temperatures (T=113K) . . . 37

6 Comparison of RT vs CT 42

7 Conclusion 52

List of Figures

1 AF-647 absorption/emission spectra. [1] 2
2 Ernst Abbe Diffraction Limit.[2, 3] 3
3 Airy disk. [4] 4
4 PSF of a conventional light microscope. The PSF of a conventional microscope is displayed by its xz and xy cross-sections. The intensity profile in the focal plane is known as the Airy disc. The distance between its first two minima is $1.22\lambda/NA$. [5] 5
5 Scetch of the main principle how a confocal microscope is structured. 6
6 Diagram of the design of a STED device. The double laser design allows for excitation and stimulated emission to be used together for STED. [6] 7
7 Excitation spot (2D, left), doughnut-shape de-excitation spot (center) and remaining area allowing fluorescence (right). [7] 7
8 The principle of single molecule localization microscopy. The majority of emitters get switched off and images are taken of emitters that stay in the on-state. This increases the accuracy of the position fo single, non-overlapping emitters. Based on the collected data a super-resolved image is reconstructed. [8] 9
9 Cut-away view of the cryostat.[9] 12
10 Schematic overview of different stand-alone Cryo stage and cryostat designs for Cryo Fluorescence Microscopy. (a) Cryo stage design for an inverted microscope setup. (b) Cryo stage for an upright microscope configuration with an autonomous LN2 cooling mechanism. (c) Vacuum insulated cryostat.[10] 12
11 Cut-away view of the cryostat. 13
12 Thermal conductivity of various materials. Oxygen-free copper definitely stands out in thermal conductivity with a factor of 1000 compared to stainless steel. [11] 14
13 14
14 The sampleholder made of oxygen-free copper and magnetic steelplate to hold the sample inside the sampleholder. 15
15 Cut-away picture of the sample holder. The only thermal connection between dye and sample holder is the magnetic plate. Plans for future experiments are already made to replace the EM-grids with coverslips. 16
16 Oxygen-free copper clips (a) and Oxygen-free copper plate and attached oxygen-free copper clips (b). 17
17 The laserpath for alternating polarization imaging. The beam splitter is used inversely in this project to create one path out of two pathes. Additionally one half-wave plate is placed in the path of laser I before the beam splitter and one aperture before both pathes enter the telescopic lense for alignment-purposes. 18

18 Thorlabs CCM1-PBS251/M Beamsplitter. 19
19 The mirror system for aligning two lasers in the same path.L1, L2 label the two red lasers. M1-M8 label the adjustable mirrors. A aperture for alignment purpose. HW half-wave plate to change the polarization of the laser beam 1. B labels the beam splitter and T the telescopic lense. 20
20 The shematic of the cryo fluorescence microscope. The laser beams (two red lasers) come from the Laser-source and first enters a cleanup filter (CF), then goes through the Mirror-system (described in the section above) to put both lasers in one path. The laser light then gets expanded by a telescope (T) and focused via achromatic lense (AL) on the back focal plane of an air objective. The ensure that the path of the laser light enters the center of the air objective an adjusting mirror (AM) and a dichroic mirror (DM) were needed. The sample gets excited via the laser light and emits fluorescence, which gets collected by the objective again and sent through the emission filter (EF). In the last step the collected and filtered fluorescence gets focused onto a SCMOS camera via a tube lens (TL). 21
21 The heavy cryostat standing on the x,y stage. Below the stage the detection path is visible. The cryostat and the setup including the wide field epi-fluorescence microscope are all custom built within this project. 22
22 Working principle of the custom made device for triggering the two lasers separately with a time delay equal to the exposure time of the lasers. (By Dipl.Ing. Martin Förser) 23
23 The custom built device to trigger two lasers separately with different possible modes. 24
24 Comparison of the vacuum decrease and dependency on which length of hose is used. 25
25 Cut-away view of the cryostat and positioning of the temperature-probes. 27
26 This picture shows how the temperature probe is attached on the copper-plate, to guarantee accurate sensoring and mapping of the temperature input. 27
27 The orange line shows the decrease in temperature of the copper plate and the blue line shows the temperature decrease of the sample holder. The temperature decrease in the first 10-15 minutes goes rapidly, then increases rapidly $\approx 30 degrees$, and decreases very slowly till equilibrium at $\approx 100 minutes$. 28
28 Comparison at t=0s and t=300s of AF-647 at RT. Even within the short timespan of 300 seconds photobleaching is clearly visible by eye.(Scale bar: 10 μm) 32
29 Detections over time of AF-647 at room temperatures. 33

30 AF-647. To quantify the photon yield the total number of detected photons was evaluated of a single frame and a merged frame. 33
31 AF-647. The localization precision calculated of a single frame and merged. 34
32 Comparison at t=0s and t=300s of an Atto-647 dye. After 300 seconds of measurement time not a single molecule is visible by eye.(Scale bar: 10 μm) 35
33 Detections over time of Atto-647 at room temperatures. 35
34 Atto-647. To quantify the photon yield the total number of detected photons was evaluated in a single frame and merged. 36
35 Atto-647. The localization precision calculated of a single frame and a merged frame. 36
36 Comparison at t=0s and t=400s of AF-647. (Scale bar: 10 μm) . . . 37
37 Detections over time of AF-647 at cryogenic temperatures. 38
38 AF-647. To quantify the photon yield the total number of detected photons per molecule was evaluated of a single frame and a merged frame. 38
39 AF-647. The localization precision calculated of a single frame and a merged frame at cryogenic temperatures. 39
40 Comparison at t=0s and t=400s of a single spot of an Atto-647 dye. (Scale bar: 10 μm) 40
41 Detections over time of Atto-647 at cryogenic temperatures. 40
42 Atto-647. To quantify the photon yield the total number of detected photons per molecule was evaluated of a single frame and a merged frame. 41
43 Atto-647. The localization precision calculated of a single frame and a merged frame at cryogenic temperatures. 41
44 Comparison of photobleaching at room temperature ($\approx$ 20 degrees C) and cryogenic temperature($\approx$ -150 degrees C) of an AF-647 dye. (Scale bar: 10 μm) 42
45 Comparison of the number of detected photons per molecule with (a) AF647 at room temperature and (b) at cryogenic temperature within a time span of 400 seconds. 43
46 Comparison of the number of detected photons per molecule with clustered frames with (a) AF647 at room temperature and (b) at cryogenic temperature within a time span of 400 seconds. 43
47 AF-647. Comparison of the localization precision of a single frame with (a) AF647 at room temperature and (b) at cryogenic temperature within a time span of 400 seconds. 44
48 AF-647. Comparison of the localization precision of a merged frame with (a) AF647 at room temperature and (b) at cryogenic temperature within a time span of 400 seconds. 45

49 Comparison of room temperature (≈ 20 degrees C) and cryogenic temperature(≈ -150 degrees C) of an Atto647 dye at t=400s. (Scale bar: 10 μm) 46
50 Comparison of the number of detected photons of a single frame with (a) Atto-647 at room temperature and (b) at cryogenic temperature within a time span of 400 seconds. 47
51 Comparison of the number of detected photons of a merged frame with (a) Atto-647 at room temperature and (b) at cryogenic temperature within a time span of 400 seconds. 47
52 Atto-647. Comparison of the localization precision of a single frame with (a) Atto-647 at room temperature and (b) at cryogenic temperature within a time span of 400 seconds. 48
53 Atto-647. Comparison of the localization precision of a merged frame with (a) Atto-647 at room temperature and (b) at cryogenic temperature within a time span of 400 seconds. 48
54 Comparison at room temperature of an AF647 and and Atto647 dye at t=300s. (Scale bar: 10 μm) 49
55 Comparison at cryogenic temperature of an AF647 and and Atto647 dye at t=400s. (Scale bar: 10 μm) 49
56 On and Off-times of AF-647 at room temperature within a measurement time of $\approx 400 seconds$. 50
57 On and Off-times of Atto-647 at room temperature within a measurement time of $\approx 400 seconds$. 50
58 On and Off-times of AF-647 at cryogenic temperature within a measurement time of $\approx 400 seconds$. 51
59 On and Off-times of Atto-647 at cryogenic temperature within a measurement time of $\approx 400 seconds$. 51

1 Abstract

Fluorescence microscopy has been one of the most important tools for understanding how biological systems are organized and how they function. Over the last two decades, the resolution of fluorescence microscopy has been enhanced by the development of super resolution methods that extend the limit of optical microscopy beyond the diffraction limit, providing unprecedented levels of information on the organization of molecular networks in cells. These methods include Structured Illumination Microscopy (SIM) [12], Stimulated Emission Depletion Microscopy (STED)[13], and techniques based on the localization of individual fluorescent molecules: Photoactivated Localization Microscopy (PALM) [14] and Stochastic Optical Reconstruction Microscopy (STORM) [15], referred to collectively as Single Molecule Localization Microscopy (SMLM) techniques. Super-resolution methods usually involve the use of chemical fixation, which has been shown to introduce artefacts that can be visible at the resolutions achieved [16]. An alternative to chemical fixation is cryofixation, which is a superior structural preservation method, but requires to preserve the specimen under cryogenic temperatures during the measurement, which requires a big adaption of the experimental set-up. Favorably, cryogenic temperatures slow down the photobleaching of fluorophores, which has the potential to improve the resolution. In this work, after a short introduction about fluorescence super resolution microscopy, the main topic will be how we built a setup for super resolution microscopy at cryogenic temperatures. After that, preliminary measurements with fluorescent dyes AF-647 (Alexa Fluor) and Atto-647N will be shown and discussed how their photophysical properties are affected by low temperatures.

2 Introduction

2.1 The Fluorophore-Fluorescence

A fluorophore is a fluorescent chemical compound that can re-emit light upon light excitation. Fluorophores can be used as a fluorescent dye, that can be used as a marker in fluorescence microscopy for proteins, tissue and cells. The fluorophore absorbs light energy of a specific wavelength and re-emits light at a longer wavelength (this difference is called the Stokes-Shift Figure 1). The absorbed wavelengths, energy transfer efficiency, and time before emission, depend on both the fluorophore structure and its chemical environment, as the molecule in its excited state interacts with surrounding molecules. Wavelengths of maximum absorption ($\approx$ excitation) and emission are the typical terms used to refer to a given fluorophore, but the whole spectrum may be important to consider. The excitation wavelength spectrum may be a very narrow or broader band, or it may be all beyond a cutoff level. The emission spectrum is usually sharper than the excitation spectrum, and it is of a longer wavelength and correspondingly lower energy. Excitation energies range from ultraviolet through the

visible spectrum, and emission energies may continue from visible light into the near infrared region. A fluorophore can repeatedly undergo the fluorescence process(in theory, indefinitely). In reality, however, the fluorophore's structural instability during the excited lifetime makes it susceptible to degradation. High-intensity illumination can cause the fluorophore to change its structure so that it can no longer fluoresce. This is called photobleaching and the fluorophore can no longer be detected.

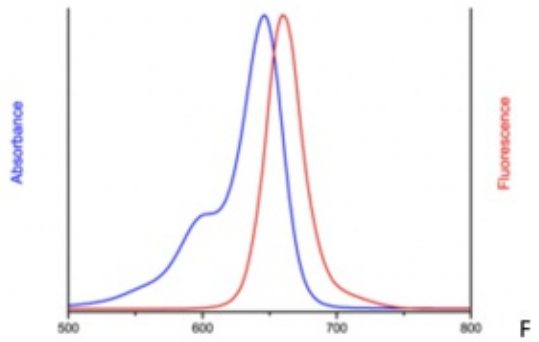

Figure 1: AF-647 absorption/emission spectra. [1]

2.2 High resolution Microscopy

The optical microscope, also referred to as a light microscope, uses visible light (visible to the human eye wavelengths from 380-740 nanometers) and a system of lenses to generate magnified images of small objects. However no matter how perfectly lenses are made, the resolution of a light microscope is physically limited by the diffraction of light, restricting it to about half the wavelength along the lateral plane and even less in the axial direction. This was first described by Ernst Abbe in 1873 [2]. In this section we will talk about the boundary of the diffraction limit, and several approaches to circumvent it will be introduced.

2.2.1 The Diffraction-Limited Resolution of Light Microscopy

The highest achievable point-to-point resolution that can be obtained with an optical microscope is governed by a fundamental set of physical laws that cannot be easily overcome by rational alternations in objective lens or aperture design. These resolution limitations are often referred to as the diffraction barrier. The diffraction limit of resolution restricts the ability of optical instruments to distinguish between two objects separated by a lateral distance less than approximately half the wavelength of light used to image the specimen. Ernst Abbe found in 1873 [2] that light with wavelength λ, traveling in a medium with refractive index n and converging to a spot with half-angle θ will have a minimum resolvable distance of d:

$$d = \frac{\lambda}{2nsin\theta} = \frac{\lambda}{2NA} \tag{1}$$

, where $nsin\theta$ is called the numerical aperture NA. The numerical aperture of an optical system is a dimensionless number that characterizes the range of angles over which the system can accept or emit light. In microscopy it is commonly used to describe the acceptance cone of an objective. So if we consider a numeric aperture of 1 (modern optics reach a NA of 1.4-1.6) and take as an example green light, which has the wavelength of around 500nm, the Abbe limit is $\approx d = \frac{\lambda}{2} = 250nm$, which is small to most biological cells ($\approx 1\mu m - 100\mu m$), but large compared to viruses(100nm), proteins(10nm) and less complex molecules. In figure 2 we can see a graphical explanation of this.

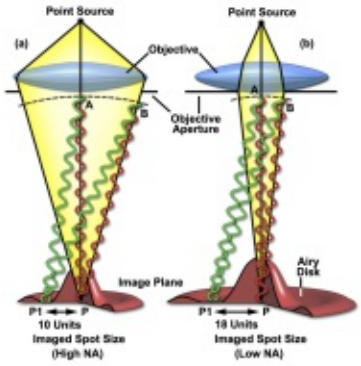

Figure 2: Ernst Abbe Diffraction Limit.[2, 3]

The objective has a finite numeric aperture, it only collects a part of the light emitted from the sample, and the light (acting as an electromagnetic wave) will interfere when it gets focused into a single point in the image plane. As a result it is not possible to focus the light of a dimensionless point emitting source into an infinitely small spot in the image plane and a bigger sized blurred spot occurs. The 3D intensity profile of this blurred spot defines the point spread function (PSF), which describes in general the response of an imaging system to a point source or point object. The degree of spreading of the point object is a measure for the quality of an imaging system. In the focal plane, the diffraction pattern is also known as the *Airydisk*. The Airy disk (figure 3) can be observed as a bright region in the center together with a series of concentric rings of decreasing intensity around it.

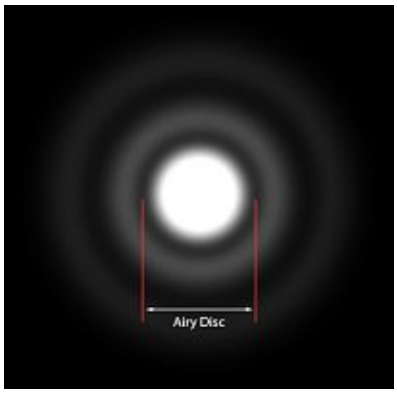

Figure 3: Airy disk. [4]

The size of the central spot in the Airy pattern is related to the wavelength of light and the aperture angle of the objective.

2.3 Single fluorescent molecule detection

Due to the diffraction limit, single molecules are not possible to detect with conventional optical microscopy. Nevertheless, there have been different efforts for decades to circumvent this resolution limit. The detection of single fluorescent molecules at cryogenic temperatures started in 1989, where single molecules were detected for the first time by W.E.Moerner [17], who observed the narrow-line features in the absorption spectrum of crystalline samples. The samples were kept at liquid helium temperatures (4K). In 1990 M.Orrit and J. Bernard [18] detected single fluorophores through their emission spectrum with a much higher signal-to-noise ratio, also at a temperature of 4K. Due to the fact that single molecules are nanometer-sized particles, this ended the time of measuring physical entities in ensemble average and the era of single molecule spectroscopy and microscopy started.
The possibility of detecting single molecules provides a direct access to studying photophysics on the molecular level. In the early 1990's behaviors like blinking and photoswitching were discovered, which led to the later application of single-molecule detection to super resolution microscopy. Also an enormous step forward was the discovery of fluorescent proteins, in particular the green fluorescent protein (GFP), which can be photo-switched.[19] The photoswitchable fluorescent proteins made localization-based super resolution techniques possible with intrinsically expressed fluorophores in living cells.

2.3.1 Confocal Microscopy

In Confocal Microscopy the diffraction limited resolution can be improved by a factor of $\sqrt{2}$.[20] In contrast to a conventional light microscope, where the entire specimen gets illuminated at the same time, in confocal microscopy small fractions(point illu-

mination) of the specimen are illuminated at every moment. Laser light is focused onto a defined spot, which leads to emission of fluorescent light exactly at this point. A pinhole is placed inside the optical pathway to eliminate signals that are out of focus. The fluorescence signals from the illuminated spot enter the detector. The illumination beam has to be scanned point to point across the entire specimen, because only one point in the sample is illuminated at a time. In principle, by decreasing the size of the pinhole, the point-spread-function(PSF) size can also be reduced, resulting in a higher resolution by a maximal factor of $\sqrt{2}$.

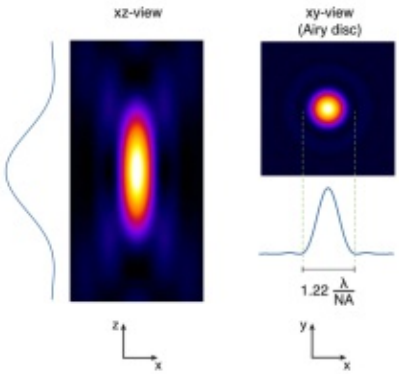

Figure 4: PSF of a conventional light microscope. The PSF of a conventional microscope is displayed by its xz and xy cross-sections. The intensity profile in the focal plane is known as the Airy disc. The distance between its first two minima is $1.22\lambda/\mathrm{NA}$. [5]

This increased resolution is at the cost of decreased signal intensity, so long exposures are often required. Another point is that the $\sqrt{2}$- resolution improvement won't be reached in practice, therefore the purpose of using the pinhole is basically to suppress the background for realizing three-dimensional sectioning, but not improving the resolution.

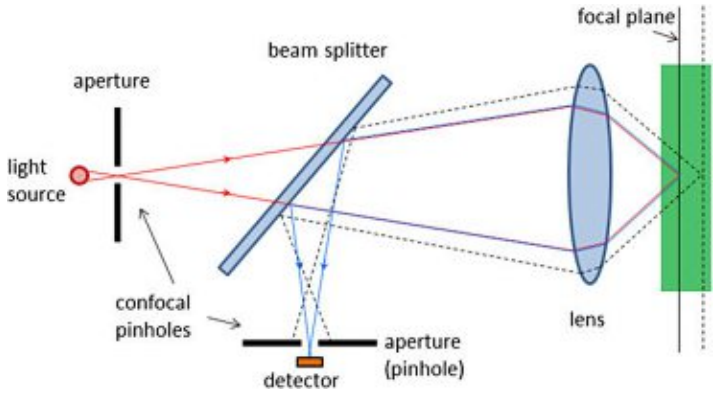

Figure 5: Scetch of the main principle how a confocal microscope is structured.

2.3.2 Structured Illumination Microscopy (SIM)

The point like illumination spot can be extended to a spatial modulated structured illumination pattern to excite fluorescence. The fluorescent sample gets illuminated by a periodic stripe pattern, that is also diffraction limited. The interference of the illumination pattern and the sample structure generates Moire patterns, with which additional information of the picture can be introduced. The phase of the stripe pattern gets shifted through a full cycle in five steps and rotated by 60 degrees in three steps. The resulting 15 images get post-processed and can be reconstructed with a doubled resolution in the lateral direction. The concept of SIM was developed by M. Gustafasson [12] as Structured Illumination Microscopy in 2000.

2.4 Super resolution microscopy

Super resolution microscopy comprises several techniques, that allow to acquire images with a higher resolution than the one imposed by the diffraction limit. These techniques achieve a typical lateral resolution of several tens of nanometers, which is one order of magnitude below the Diffraction Limit of Ernst Abbe. Super resolution enables direct observation of samples on the nanometer scale, and has resulted in numerous applications and discoveries in the chemical, biological, and medical sciences. In this section the following techniques will be discussed:

- Stimulated emission depletion microscopy(STED)
- Single molecule localization microscopy(SMLM)

2.4.1 Stimulated emission depletion microscopy(STED)

As we discussed before, due to diffraction the excitation laser can't be focused into an infinitely small spot, so the illumination extent is given by the size of the PSF, which is typically $\approx 200 - 500nm$. When illuminating a sample with this PSF, all

fluorophores in the focal volume will be excited and will emit fluorescence at the same time, so structures within the diffraction limited spot can't be separated. By using STED an enhanced resolution can be achieved via minimizing the area of illumination due to deactivation of fluorophores of a special region.

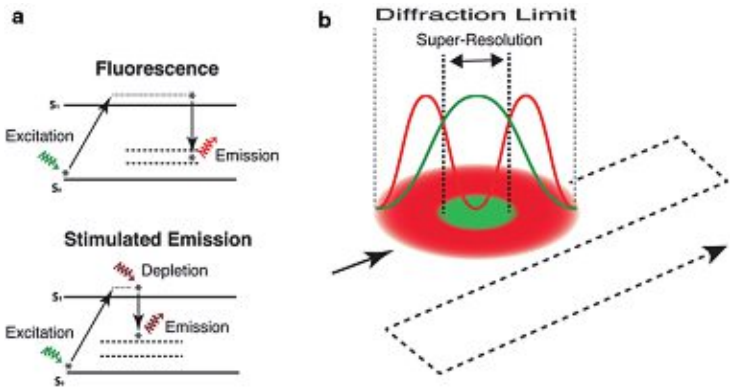

Figure 6: Diagram of the design of a STED device. The double laser design allows for excitation and stimulated emission to be used together for STED. [6]

STED functions by depleting fluorescence in specific regions of the sample while leaving a center focal spot active to emit fluorescence. An additional laser spot with a doughnut-like intensity profile is overlapped with the confocal illumination spot. This doughnut spot has zero intensity in the middle and its wavelength matches the transition energy of the fluorophore from the excited state to one of the vibrational energy levels in the ground state.

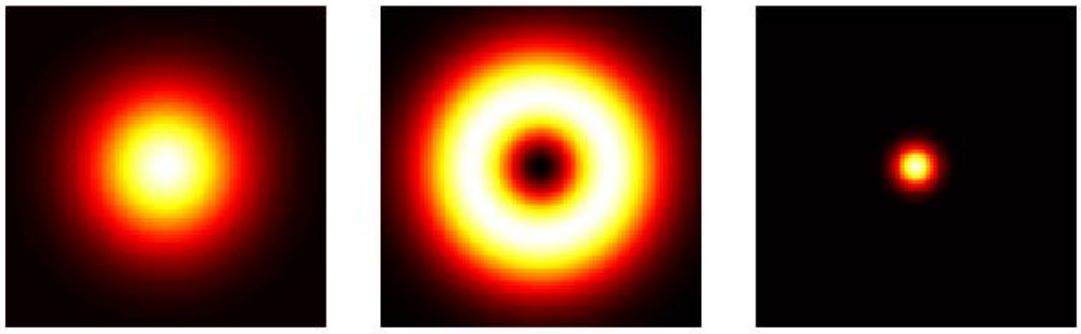

Figure 7: Excitation spot (2D, left), doughnut-shape de-excitation spot (center) and remaining area allowing fluorescence (right). [7]

The size of this zero center is typically by one order of magnitude smaller than the size of the confocal volume, which determines the resolution of the STED. This super-resolution can only be achieved when the used dyes are STED-compatible. To

allow for STED analysis of biological systems, the dyes and laser sources must be tailored to the system.

2.4.2 Single molecule localization microscopy(SMLM)

Single molecule localization microscopy (SMLM) achieves higher resolution below the diffraction limit due to localization of single fluorescent molecules, which results in the potential to quantify the spatial organization of molecules in cells. Since single fluorophores typically have a size of $\approx 1nm$ and fluorescent proteins $\approx 4nm$, they act as point emitters. Due to the diffraction limit, the imaged spot is larger than the point source and if a biological sample is labeled with several fluorophores at a high concentration the point spread functions of the fluorophores overlap, when they emit at the same time. To localize single molecules the emission profile has to exhibit minimal overlap in each image. The centroid position of each identified molecule is statistically fitted by a Gaussian function. To overcome this problem the emission of fluorescence of single fluorophores has to be temporally separated, which can be achieved via different approaches. Photoactivated localization microscopy (PALM) uses photoactive fluorescent proteins and was first implemented in 2006 by E.Betzig [21]. Another method to temporally separate fluorescent signals was published by X. Zhuang [22], named stochastic optical reconstruction microscopy (STORM). The majority of emitters get switched off and images are taken of emitters that stay in the on-state. By imaging and fitting single emitters to a sub-diffraction limited spot over thousands of single images an overall image can be created that contains the information of the composite reconstruction of all identified emitters. The resolution is determined only by the localization accuracy.

However, given an isolated emitter, one is able to determine its location with a precision only limited by its intensity according to the following equation:

$$\Delta loc \approx \frac{\Delta}{\sqrt{N}} \tag{2}$$

where Δloc is the localization precision, Δ is the FWHM(Full Width at Half Maximum) of the PSF and N is the number of collected photons. So we can see that the localization accuracy mostly depends on the detected number of photons N per molecule. In practice, several hundred photons can be detected from single molecules in a typical integration time of tens of milliseconds, which results in a localization accuracy of several tens of nanometers in the lateral plane.

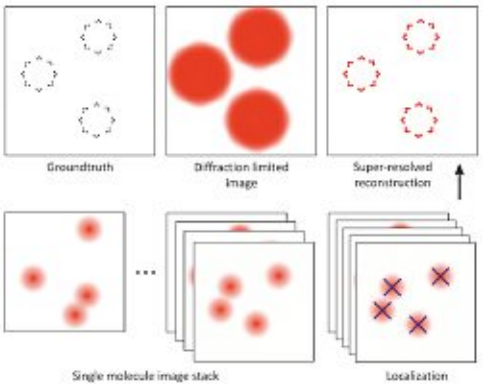

Figure 8: The principle of single molecule localization microscopy. The majority of emitters get switched off and images are taken of emitters that stay in the on-state. This increases the accuracy of the position fo single, non-overlapping emitters. Based on the collected data a super-resolved image is reconstructed. [8]

Although super-resolution microscopy techniques seem to have theoretically no limitation in resolution, photo-bleaching, thermal drift and molecule fixation restrict the maximum achievable resolution to several tens of nanometers.

2.5 Cryo Super Resolution Microscopy (Cryo SMLM)

Almost half a century ago liquid nitrogen cooled and temperature regulated sample stages for light microscopes have been developed to study along applications in the biomedical field. Cryo Fluorescence Microscopy is becoming more and more popular in the field of single molecule localization [9]. The advantages of Cryo super resolution microscopy are many: Photo-bleaching can be strongly suppressed at cryogenic temperatures, which results in an enhanced photo-stability of the fluorophores, increasing the photon numbers detected from a single molecule [23]. As discussed before, an increase in the number of photons goes hand in hand with localization accuracy. A major advantage is that most fluorophores have narrower emission and absorption spectra at low temperatures, reducing spectral overlap and allowing better multicolour imaging [24]. Current results show that by cooling a sample from room temperature down to liquid nitrogen temperatures, the photo-stability of dyes can be enhanced by more than 100 fold, which then results in an improvement in localization precision greater than 10 times [25]. Another advantage is the superior structural preservation of the sample. Since fluorophores are dipole emitters, the dipole will be frozen at cryogenic temperatures. This supposes a new challenge that might be translated into an advantage, since it can be used to differentiate between neighboring molecules. There are several challenges too: Under cryogenic conditions, fluorophores are far more likely to be excited to a dark state, from which they are not able emit fluorescence [26]. This results in a significant decrease in overall signal from the sample. However, these characteristics are not known for all fluorophores and

more research is being done to optimize fluorophores for cryogenic imaging. Another exciting observation is that "blinking" of fluorophores still occurs under cryogenic conditions, allowing cryogenic super resolution microscopy [27]. Currently, the major drawback in Cryo Fluorescence Microscopy is the relatively low NA of air objectives that can be used for cryogenic purposes, because in contrast an oil immersion objective can go NA of ≈ 1, while current available air objectives reach ≈ 0.7. Some advances have been made in the design of immersion objectives and immersion fluids that work at very low temperatures [28]. However the low NA objective will be compensated with an increase in photon numbers per molecule. Vibrations or bubbling of the cryogen can be directly transmitted to the sample, so the cryostat itself plays a very important role to isolate the sample from vibrations. Also vibrations that arise from the vacuum pump and other external devices used to decrease the temperature play a very important role. The loading to the cryostat represents an issue due to the fact that the sample needs to be vitrified before the experiment using rapid freezing techniques. Therefore cryostats must provide the possibility to transfer frozen samples below the glass transition temperature of water ($\approx 135K$) to prevent ice crystal formation in the sample.

For this project a new Cryo system was developed and will be discussed in the following sections (based on the one described in [5]). In the first part, the design of the cryostat will be explained and shown, including all the issues we faced and tried to solve. In the second part, measurements with AF-647 and Atto-647 at room temperature and at cryogenic temperatures will be analyzed.

3 Cryostat design

In this section the basic design and selection of certain materials will be discussed. For single molecule microscopy the cryostats are typically designed to be vacuum-insulated to provide high thermal and mechanical stability. The sample is attached to a cold substrate, which is kept at cryogenic temperatures (CT) by a static cryogen reservoir. One drawback of this design is that any vibration or bubbling of the cryogen will be directly transmitted to the sample, causing considerable mechanical instability. This will be discussed in detail in the following chapters.
Another parameter to consider, is the choice of cryogen. Although the use of liquid He (temperature of 4K) provides a more stable flow, less bubbling and a lower temperature, compared to liquid nitrogen (temperature of 78K), the operational cost would not stand in relation to its purpose. An issue of the concept of a closed cryostat is that the sample can't be transferred to the cryostat, when it is already vacuum-insulated, so it has to be loaded at room temperature and then cooled down. This makes the study of vitrified samples and the preservation of examined samples nearly impossible. There exist different implementations for Cryo Super Resolution FM, like shown in figure 10. In (a) a cryo stage design for an inverted microscope setup is shown. Cooling is achieved by pumping liquid nitrogen (LN2) through the Cryo stage. Imaging is performed through a long working distance air objective which is separated from the cryo environment by a glass window and kept at ambient temperature. A cryo stage for an upright microscope configuration with an autonomous LN2 cooling mechanism can be seen in (b). The objective is dipping into the cold nitrogen atmosphere inside the Cryo stage. An air objective with a long working distance is required to avoid heat transfer to the sample. Additional cooling of the objective allows reducing the working distance and thus an objective with a larger NA can be used to increase resolution. Full integration of the objective into the Cryo stage and immersion imaging under Cryo conditions have been shown with a design of overall similar principle. The Cryo stage design for a vacuum insulated cryostat can be seen in (c). Temperature stability and range (also liquid helium (LHE) cooling possible) is increased compared to Cryo stages as shown in (a) and (b), but the implementation of a sample transfer mechanism is very complicated. Higher NA air objectives can be used if placed inside the cryostat, but the NA is limited to < 1.0 due to the incompatibility of Cryo immersion with vacuum. [10] In this project we are using the typical design for cryo stages (a), that consist of an insulated liquid nitrogen cooled chamber, that can be opened for sample exchange, and a long working distance air

objective that is kept at room temperature via separation by a glass window (Figure 9).

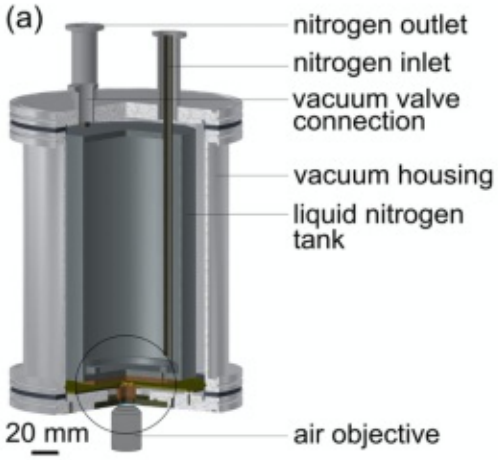

Figure 9: Cut-away view of the cryostat.[9]

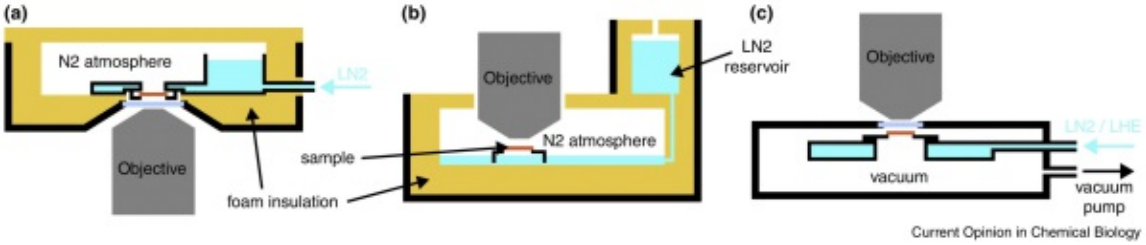

Figure 10: Schematic overview of different stand-alone Cryo stage and cryostat designs for Cryo Fluorescence Microscopy. (a) Cryo stage design for an inverted microscope setup. (b) Cryo stage for an upright microscope configuration with an autonomous LN2 cooling mechanism. (c) Vacuum insulated cryostat.[10]

3.1 Coupling of cooling components

An schematics cut-away view of the cryostat can be seen in figure 11. The first instance of the cryostat is the tank, which gets filled with liquid nitrogen. The tank is made out of stainless steel, the drawback in this case is, that stainless steel is a relatively low thermal conductor at cryogenic temperatures, compared to oxygen-free copper (figure 12 shows this in detail).

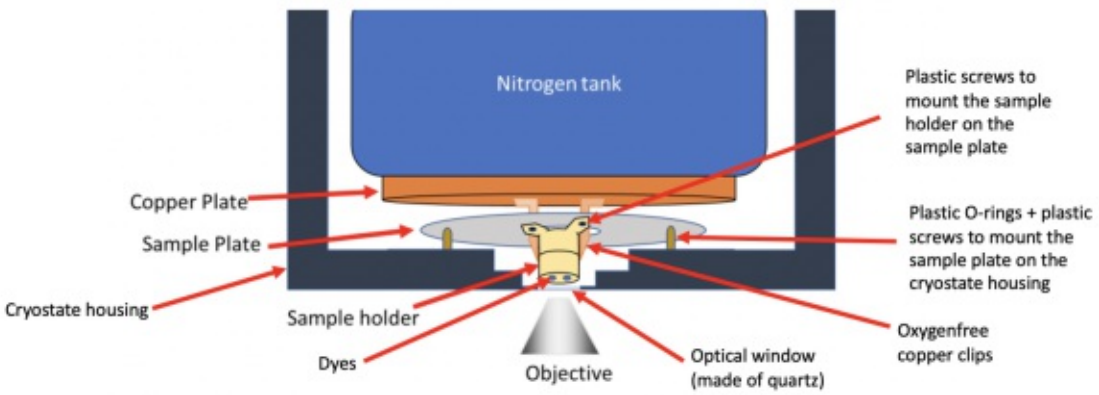

Figure 11: Cut-away view of the cryostat.

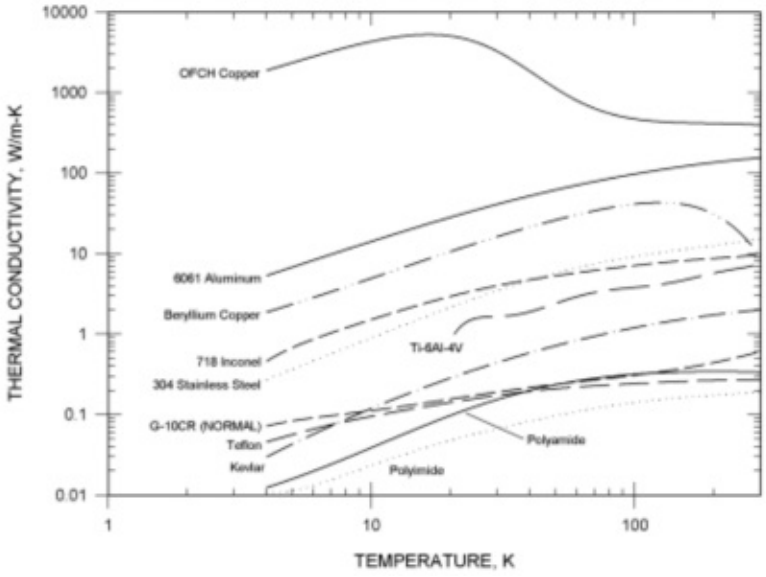

Figure 12: Thermal conductivity of various materials. Oxygen-free copper definitely stands out in thermal conductivity with a factor of 1000 compared to stainless steel. [11]

A disc made out of oxygen-free copper is attached to the surface of the stainless-steel cylinder. This disc is in direct thermal contact with the sample holder, although mechanically decoupled from it. Additionally, to fill any surface irregularity between the disc and the stainless steel cylinder a thin indium sheet is sandwitched and seamless heat transfer is guaranteed. Indium is a very good thermal conductor and very soft at room temperature, so it is very suitable for seamless heat transfer (figure 13).

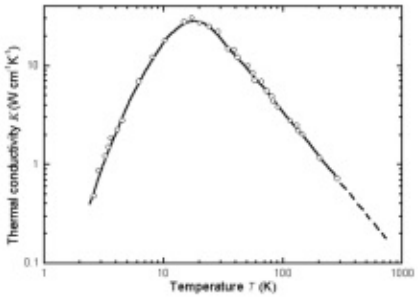

(a) Thermal conductivity of Indium. [29]

(b) Real picture of an Indium sheet.

Figure 13

The sample holder consists of two parts, one is attached to the sample plate and another one (figure 14) that is magnetically attached to the upper one. The sample mount is fixed on the sample plate, wich is fixed on the bottom of the vacuum housing using spacers and screws. The spacers and screws have very low thermal conductivities at cryogenic temperatures and minimize the heat loss due to this created temperature bridge. Due to the fact that while cooling the cryostat, the tank undergoes enormous thermal drift and mechanical vibrations, the sample plate decouples from the sample mount and the sample holder that is connected to it via integrated magnets, from the cryogen and its vibrations. Another benefit that arises through the sample plate is that it provides a steady place to fix the sample. If the sample-holder gets attached to the copper clips without the sample plate it seems really hard to find a focused spot without being off the coordinates or any tilting. As shown in figure 16 the sample-holder has four holes that are made for placing EM-grids, which contain the sample. The sample holder can also be used with round coverslips (12mm diameter)

Figure 14: The sampleholder made of oxygen-free copper and magnetic steelplate to hold the sample inside the sampleholder.

On top of it a magnetic plate is placed to hold everything together. However this turned out to have several issues:

- The surface area of the holes can't be polished or cleaned properly, so background fluorescence arises, which is difficult to distinguish from the fluorescence of the dye.
- The thermal connection of the EM-grids and sample holder can't be guaranteed, because the cryostat is made to be upside down so gravity forces the EM-grids to fall on the magnetic plate (figure 15). The temperature probe is only attached on the sample holder, so the temperature of the EM-grid is unknown. Due to the difficulties of using EM-grids coverslips were used for this thesis. Fused silica coverslips seem to be ideal, because they can be cleaned easily via burning with a Bunsen Burner ($\approx 1200°C$) due to the high melting point of silica ($\approx 2000°C$),

which ensures to remove all fluorescent impurities on the silica coverslip without melting it.

- Due to the fact that the EM-grids are not attached tightly on the sample holder, the temperature conduction is not guaranteed to full extend.

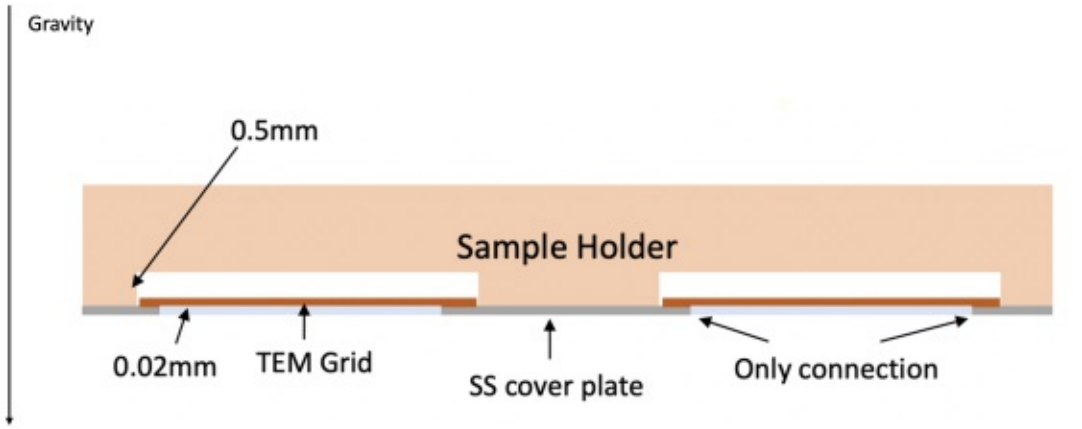

Figure 15: Cut-away picture of the sample holder. The only thermal connection between dye and sample holder is the magnetic plate. Plans for future experiments are already made to replace the EM-grids with coverslips.

In the beginning of this project copper braids connected the copper-plate with the sample-holder. The main reason for this was that the braids should decrease the remaining vibrations that are created by thermal drift and mechanical vibrations. However in this project they got substituted by copper clips (figure 16), because they support the temperature connection a lot better and can be attached and tighter to the sample holder than copper braids. The drawback of this design is, that the oxygen-free copper clips possibly transport mechanical vibrations that arise from the cryogen more than copper braids. However copper braids are also getting solid at cryogenic temperatures and no significant increase in vibrations was observed. In every case attention has to be paid that the copper clips/braids don't touch a single spot the sample plate, because this would result in a large temperature bridge and thermal insulation decreases. The opening at the bottom of the cryostat ,meant for sample loading and exchange, is closed by a window disc and sealed via a Viton O-ring. A 0.5mm optical quartz window is glued to it, through which the sample can be observed. The low thermal expansion coefficient of quartz makes it ideal for mirrors and optical flats. It is transparent to wavelengths from around $0.2 - 3.5\mu m$ and has a good thermal shock resistance. When the window disc is attached to the cryostat, there remains a $\approx 0.5mm$ distance between the sample and the inner side of

(a) Oxygen-free copper clips.

(b) Oxygen-free copper plate and attached oxygen-free copper clips.

Figure 16: Oxygen-free copper clips (a) and Oxygen-free copper plate and attached oxygen-free copper clips (b).

the optical window. This design is made for the use of air-objectives with a working range of above $\approx 1.2mm$.

3.2 Measurements at cryogenic temperatures

Fluorescent dyes on a dry mounting don't require rapid freezing techniques to undergo the vitrification point of water as fast as possible, because no water molecules are located on the mounting. Due to the fact that in this work only dyes on dry mountings were examined it is not necessary to load the samples at cryogenic temperatures into the cryostat. However there are three situations in which samples need to be loaded into the cryostat at cryogenic temperatures.

- The sample is prepared in a hydrated mounting medium and is pre frozen.
- Multiple samples need to be examined in a series at cryogenic temperatures.
- Correlative measurements with cryo-EM are required.

To make the loading of cells or any kind of dyes, that contain water molecules possible, it has to be worked on the cooling rate of the cryostat and an extra device has to be built for opening the cryostat after it is already cooled and filled with liquid nitrogen. Sample transfer at CT has to avoid any exposure to the humid air to prevent ice condensation, and must be carried out below the glass transition temperature of water ($\approx 135K$) to avoid ice crystal formation in the sample. In this project, however, we will measure only dry samples, so there will be no need for cold sample loading.

3.3 Optical setup

In this section of the thesis the coupling of the cryostat to the microscope and the experimental steps to a complete setup will be discussed. In this optical setup, two

red lasers can be triggered independently and get aligned into one path via adjustable mirrors and a beamsplitter. The path of red laser I gets reflected by three mirrors, the red laser II by two mirrors, of 90° before they enter the beam splitter. This makes the alignment of both lasers in the same path very accurate and more precise to adjust. The beam splitter(Thorlabs CCM 1-PBS251/M) consists of two triangular glass prisms, which are glued together at their base using polyester, epoxy or urathane-based adhesives. The thickness of the resin layer is adjusted such that (for a certain wavelength) half of the light incident through one "port" is reflected and the other half is transmitted due to frustrated total internal reflection. Polarizing beam splitter use birefringent materials to split light into two beams of orthogonal polarization states. However we are using it inversely to create a setup for alternating polarization imaging. Since fluorophores at cryogenic temperatures have been reported to have low blinking, alternated polarized laser light can be used to image the dipole orientation of the fluorophore, because its dipoles are frozen.

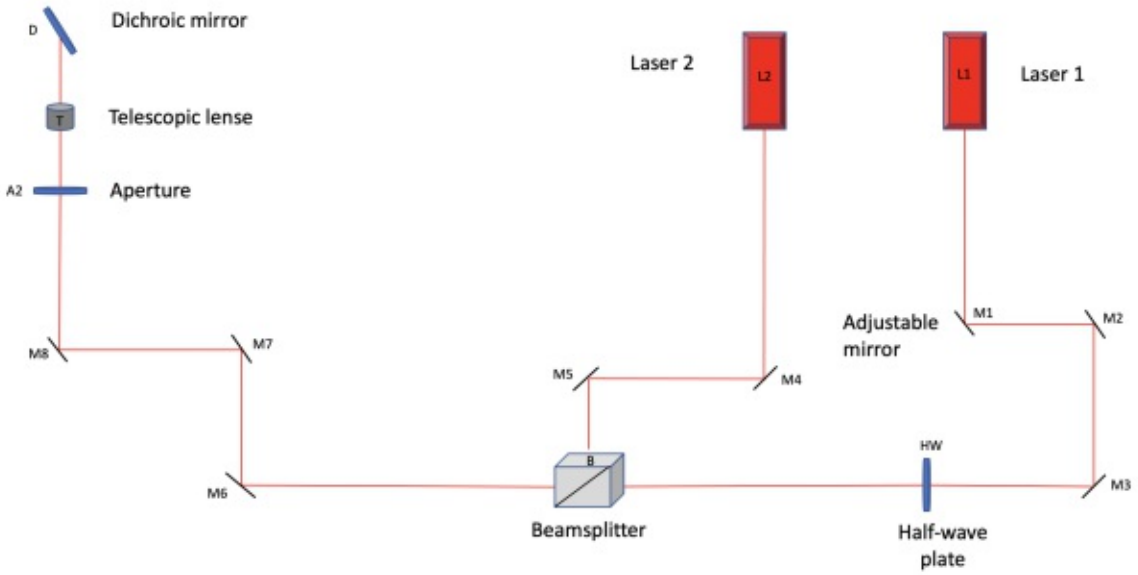

Figure 17: The laserpath for alternating polarization imaging. The beam splitter is used inversely in this project to create one path out of two pathes. Additionally one half-wave plate is placed in the path of laser I before the beam splitter and one aperture before both pathes enter the telescopic lense for alignment-purposes.

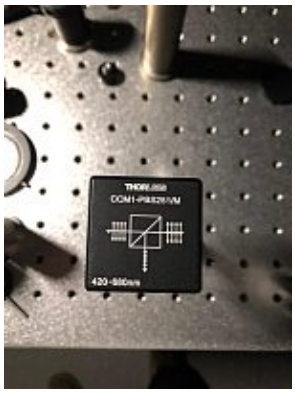

Figure 18: Thorlabs CCM1-PBS251/M Beamsplitter.

It has to be emphasized that a proper alignment of the laser paths is fundamental concerning the focus of the objective and the resulting resolution. In this project a lot of time has been spent in the perfect alignment and placing of mirrors to ensure a perfectly adaptable system of tools to align faster and with sufficient accuracy.

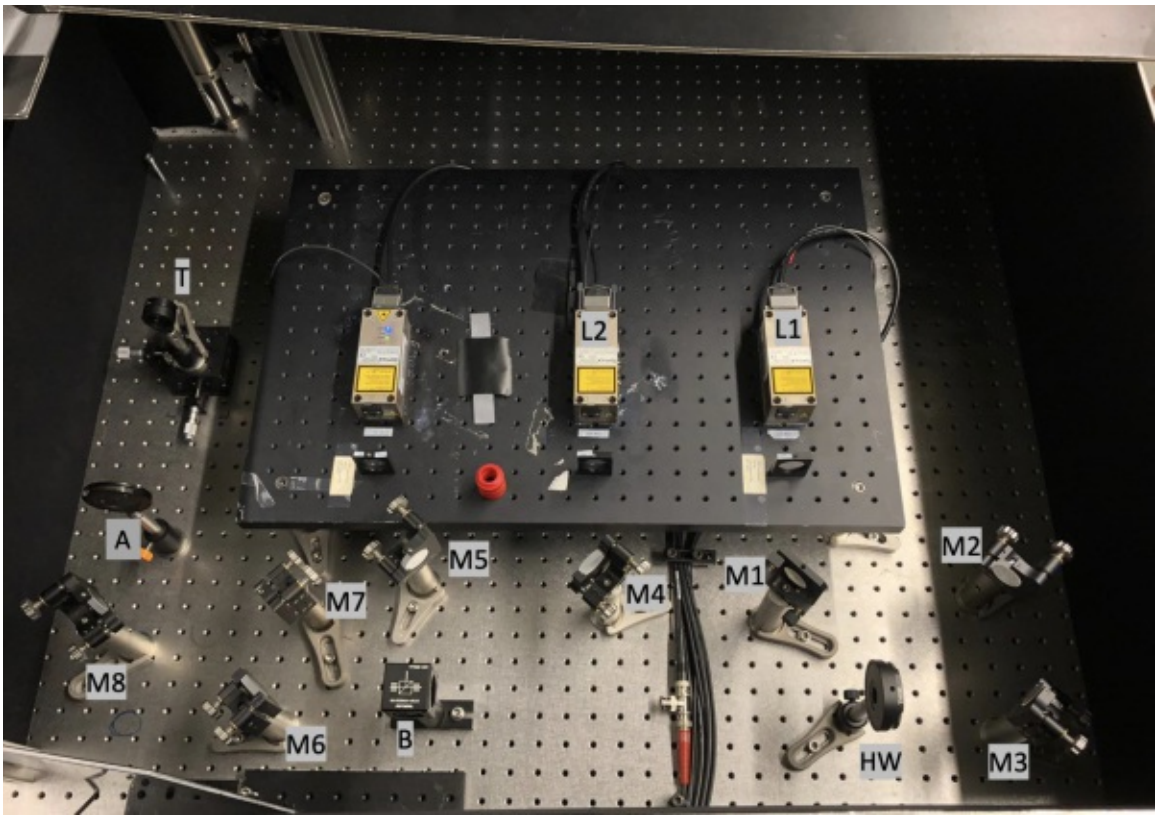

Figure 19: The mirror system for aligning two lasers in the same path.L1, L2 label the two red lasers. M1-M8 label the adjustable mirrors. A aperture for alignment purpose. HW half-wave plate to change the polarization of the laser beam 1. B labels the beam splitter and T the telescopic lense.

The cryostat is designed to be used for an inverted microscope and has a weight of $\approx 15kg$, so an additional stage is needed to guarantee precise movement in x,y-directions and mechanical stability. The stage can be moved in x, y-coordinates as shown in figure 22, via screws on the edges of the stage. Below the stage an inverted epi-fluorescence microscope was built and any objective can be attached to it (in this project an air objective is used). The objective is mounted on a vertical piezo-stage, which makes precise focusing possible. For illumination of the sample this setup is equipped with two continuous wave lasers. The laser light is sent through a clean-up filter directly at the input, then goes through the mirror and beamsplitter-system as shown in figure 19 and gets expanded by a telescopic lens. The expanded beam then gets focused onto the back focal plane of the objective by an achromatic lens and reflected on a dichroic and adjusting mirror. The sample gets illuminated by a focused spot of the objective and the fluorescence emitted from the sample gets collected from the objective again. The collected fluorescence is sent through an emission filter and focused onto an SCMOS-camera via a tube lens.

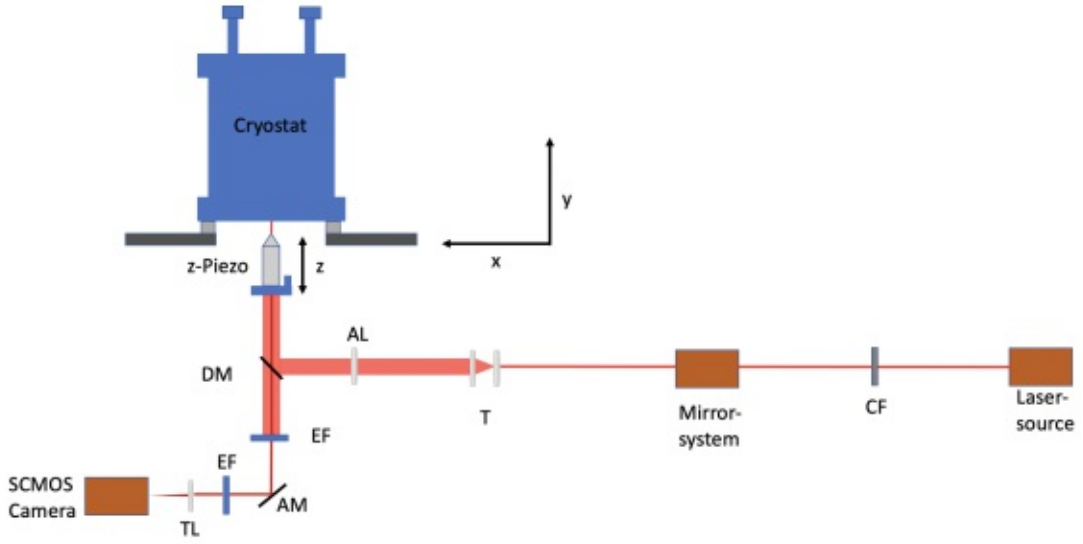

Figure 20: The shematic of the cryo fluorescence microscope. The laser beams (two red lasers) come from the Laser-source and first enters a cleanup filter (CF), then goes through the Mirror-system (described in the section above) to put both lasers in one path. The laser light then gets expanded by a telescope (T) and focused via achromatic lense (AL) on the back focal plane of an air objective. The ensure that the path of the laser light enters the center of the air objective an adjusting mirror (AM) and a dichroic mirror (DM) were needed. The sample gets excited via the laser light and emits fluorescence, which gets collected by the objective again and sent through the emission filter (EF). In the last step the collected and filtered fluorescence gets focused onto a SCMOS camera via a tube lens (TL).

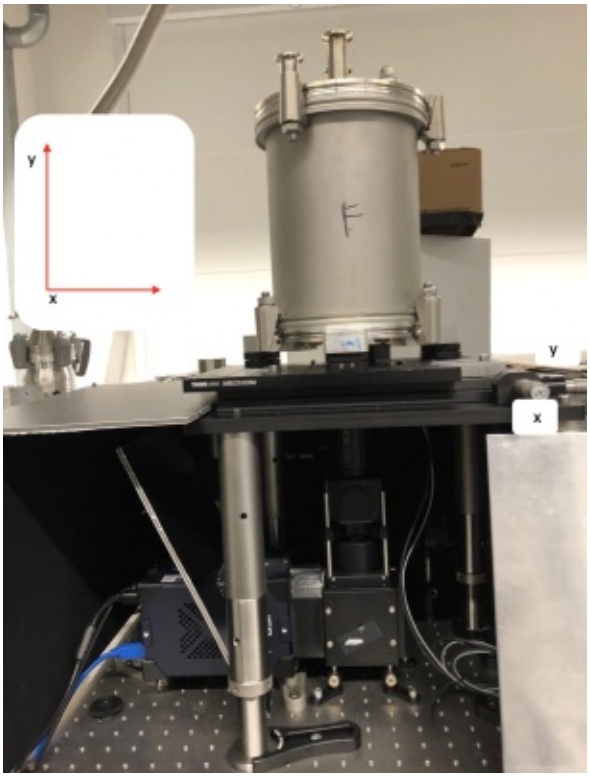

Figure 21: The heavy cryostat standing on the x,y stage. Below the stage the detection path is visible. The cryostat and the setup including the wide field epi-fluorescence microscope are all custom built within this project.

3.4 Triggering two lasers separately

The fluorophores on the sample excited with laser light emit fluorescence, which can be collected and imaged, however due to the fact that fluorophores move, they also show different dipole orientations. The probability of photon absorption is proportional to the square of the projection of the electric field onto the dipole orientation:

$$P_a \propto cos^2(\theta_a) \tag{3}$$

Where P_a is the probability of photon absorption, θ_a is the angle between the polarization of the exciting light and the absorption dipole (for instance, $\theta_{ax}$when the light is polarized along the x axis). Absorption of light is most likely, when the polarization is oriented parallel to the absorption dipole. As fluorescence is only produced when the molecule absorbs light, by varying the input polarization and detecting the fluorescence for each polarization, information about the dipole angle is obtained. For this purpose an extra device has been built together with Dipl.Ing. Martin Förser to trigger the two lasers separately. With this device it is possible to build a laser path consisting of two different polarizations that are triggered with a short time delay on each other. One can roughly conclude the mode of operation with flank-triggered

on/off-modes for the laser. Both lasers are connected to the device, to which alternated current is fed in. On the positive flank laser 1 gets triggered and on the negative flank laser 2 gets triggered, so this creates alternated triggering of two lasers with a time delay of the exposure time, that can be set manually via the National Instruments laser triggering program.

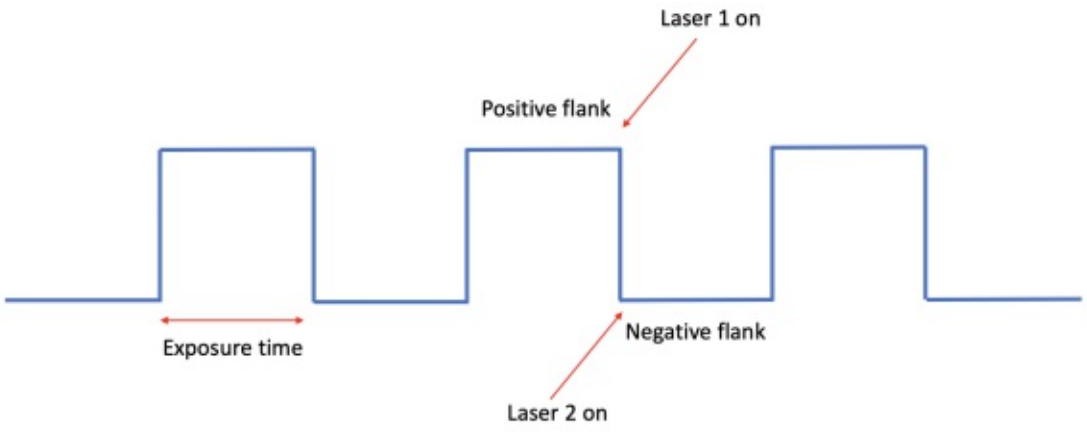

Figure 22: Working principle of the custom made device for triggering the two lasers separately with a time delay equal to the exposure time of the lasers. (By Dipl.Ing. Martin Förser)

The figure below shows the custom built device to trigger two lasers separately with different possible modes.

- Off:
  The laser that is connected to this input is turned off.
- Trigger and Toggle:
  The laser that is connected to this input can be triggered and turned off within the set exposure time. This mode is required for alternated polarization imaging.
- Trigger:
  The laser that is connected to this input can be triggered with the set exposure time.
- On:
  The laser that is connected to this input is turned on constantly.

Figure 23: The custom built device to trigger two lasers separately with different possible modes.

3.5 Installing the Piezo Controller

Focusing quality and adaption has to be as precise as possible. For this purpose a digital piezo controller (model "E-709 digital piezo controller" from Physik Instrumente GmbH Co.K) has been installed. The device comes with a range of $\approx 100nm$, which makes fine focusing possible. At this point it has to be emphasized that the stage, on which the cryostat stands, can be moved in x,y direction manually with screws precise enough to not disturb the focus. However also in z-direction rough focusing is done manually, because the $100nm$ range of the piezo controller is too low to focus through the overall range of the objective.

3.6 Installing the vacuum pump

The vacuum pump (HiCube, Pfeiffer Vacuum GmbH, Germany) plays a very important role for the cryostat, because the inner vessel is sealed into an outer vessel, which acts as the vacuum housing. Between these two vessels, a vacuum of $\approx 10^{-6}hPa$ is generated for thermal insulation. The sample and the internal components of the cryostat are located in this vacuum. This has two reasons:

- Water molecules and evaporation have to be sucked off to work in a dry environment. A dry environment plays a very important role when it comes to Cryo Super Resolution Fluorescence Microscopy, because if there are water molecules left and the sample cools down, crystallization happens and disturbs the fluorescence measurements.

- To ensure stable temperature conditions, because when liquid nitrogen gets filled in the tank the less particles that are left, the better the temperature behavior in the outer chamber. Vacuum does not transfer heat, so this also ensures the outer part of the cryostat is not cold, and there is no water condensation at the optical window.

Before filling liquid nitrogen into the tank the vacuum should reach a level of at least $\approx 10^{-4} hPa$, otherwise it won't decrease to the required level of $\approx 10^{-}6hPa$. The dependency of the length of the hose from the vacuum pump to the cryostat shouldn't be neglected. The first approach was to build a long hose and put the vacuum pump on the floor to decouple it mechanically from the system and let the vacuum pump run during measurements. The motive of this approach was to reduce the vibrations on the sample that arise through the vacuum pump. However this setup had several issues, including the longer time to build the required level of vacuum, overall loss of the vacuum due to connection points of the hose and the vibrations couldn't be erased completely even with putting a concrete block in the middle of the hose. Figure 26 shows the difference in time and levels of the vacuum comparing a shorter hose and a longer hose, when filling liquid nitrogen into the tank.

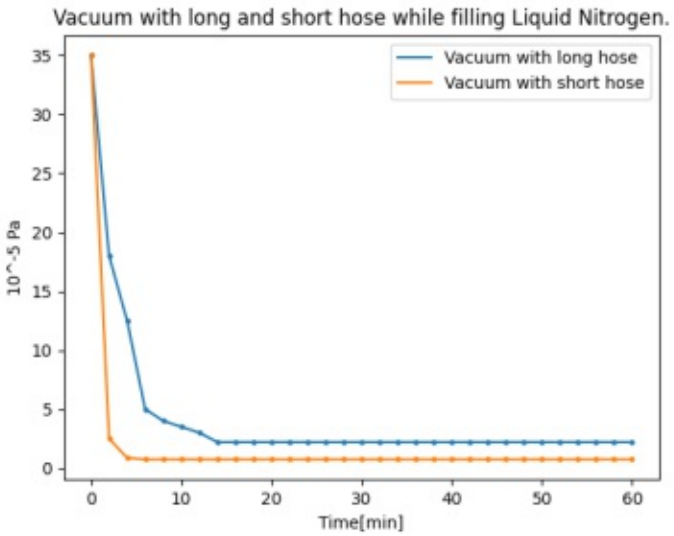

Figure 24: Comparison of the vacuum decrease and dependency on which length of hose is used.

In this project the short hose for a fast building of the required vacuum is used, because it has been shown that the hose can be plugged off from the system completely after the cryostat is cooled down to an adequate temperature. This results in zero vibrations and a stable temperature profile during the measurement process. When the cryostat is completely filled with liquid nitrogen and cooled down a stable vacuum of $\approx 10^{-}6hPa$ can be maintained for several hours even without any connection to the vacuum pump.

3.7 Installing the temperature probe

For measuring the temperature exactly thermocouple temperature probes are used. A thermocouple is an electrical device consisting of two dissimilar electrical conductors forming an electrical junction. A thermocouple produces a temperature-dependent voltage as a result of the thermoelectric effect, and this voltage can be interpreted to measure temperature. Thermocouples are a widely used type of temperature sensor. In general there exist various types of thermocouples, that are built for different temperature ranges. In this project the T-type is used. Type T(copper-constantan) thermocouples are suited for measurements in the 78K-658K range. Often used as a differential measurement, since only copper wire touches the probes. Since both conductors are non magnetic, there is no Curie point and thus no abrupt change in characteristics. They have a sensitivity of $\approx 43\mu V per Kelvin$. Note that copper has a much higher thermal conductivity than the alloys generally used in thermocouple constructions, and so it is necessary to exercise extra care with thermal anchoring type-T thermocouples. The wires that make up the thermocouple must be insulated from each other everywhere, except at the sensing junction. Any additional electrical contact between the wires, or contact of a wire to other conductive objects, can modify the voltage and give a false reading of temperature. When wire insulation disintegrates, it can result in an unintended electrical contact at a different location from the desired sensing point. If such a ”damaged” thermocouple is used, this can lead to false temperature reading.

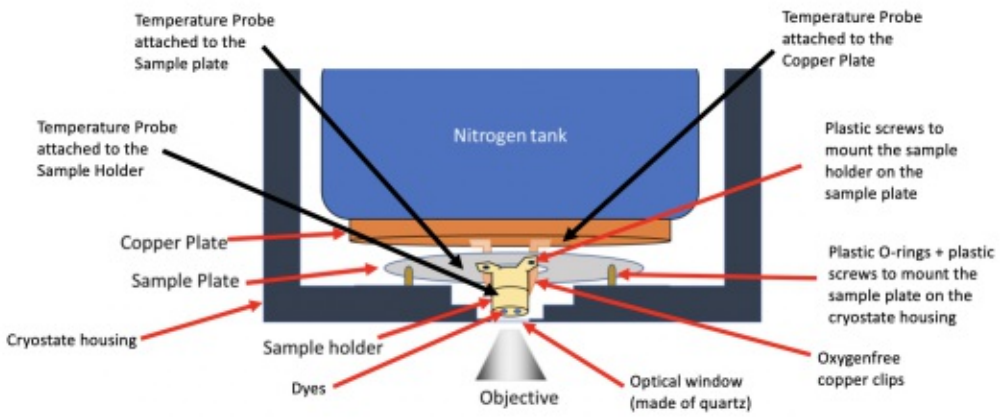

Figure 25: Cut-away view of the cryostat and positioning of the temperature-probes.

As soon as the wires are connected they measure the temperature, so in this case it has to be ensured that the wires also touch the medium they are supposed to measure. A lot of measuring errors or difficulties arised through false connection of the temperature probe onto the copper plate and the sample holder. It also has to be emphasized that measuring the temperature directly on the sample is not possible, and the temperature is measured as close as possible(at the sample holder). Heating of the sample through laser excitation has to be evaluated in future experiments. Nevertheless when reaching liquid nitrogen temperatures even if we have with slightly heating up the sample due to laser excitation, cryogenic properties won't be disturbed.

Figure 26: This picture shows how the temperature probe is attached on the copper-plate, to guarantee accurate sensoring and mapping of the temperature input.

3.8 Thermal stability

The last step before the cryo setup is going to be put into operation is to study the thermal stability of the system. For this reason multiple cooling tests have been done. As the first step the air in the cryostat was evacuated via using the turbo pump creating a vacuum of $\approx 10^{-4} hPa$. With the aim to reach a vacuum of $\approx 10^{-6} hPa$ this turned out to be the perfect moment to fill the liquid nitrogen into the inner tank. The vacuum drops down to $\approx 10^{-6} hPa$ within several minutes. The temperature on the copper plate and sample holder decrease very fast (shown in figure 27).

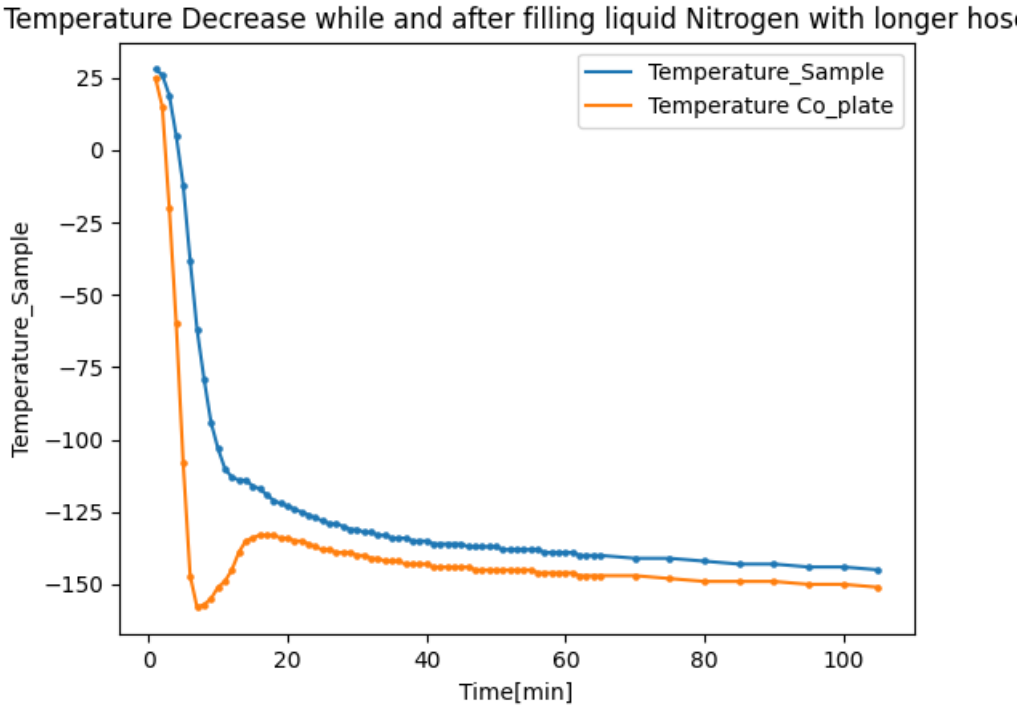

Figure 27: The orange line shows the decrease in temperature of the copper plate and the blue line shows the temperature decrease of the sample holder. The temperature decrease in the first 10-15 minutes goes rapidly, then increases rapidly $\approx 30 degrees$, and decreases very slowly till equilibrium at $\approx 100 minutes$.

The temperature drop in the first 10-15 minutes goes rapidly down to -155 degrees C on the copper plate and -115 degrees C on the sample holder. The temperature of the copper plate also rises to an extend of 30 degrees within 5-10 minutes and then slowly decreases until it reaches equilibrium at -150 degrees C after 100 minutes. The sample holder shows a much more linear behavior after the first temperature drop and decreases slowly and constantly until equilibrium at -145 degrees C in the same time the copper plate needed. This dropping-increasing-dropping behavior points out that there is some temperature-bridge inside the cryostat. This could have many reasons:

- Thermal connections with the sample plate: The sample holding plate is needed to have a perfect aligned base of the sample holder and to decouple it from the mechanical vibrations that arise from the liquid nitrogen filled tank of the cryostat. This plate is at room temperature and thermically isolated from the "cold" parts of the cryostat since it is screwed onto the cryostat outlet. If cooling down the sample plate, the cryostat outlet would also get cooled down, and this results in an enormous loss of thermal energy. As a result the screws with which the sample holder is coupled to the sample plate have to be as low thermally conducting as possible. At the moment we are using PEEK screws. PEEK screws (chemically known as Polyetheretherketone) offer a unique combination of properties for some of the most extreme applications. PEEK is classified as semicrystalline thermoplastic and high purity polymer, offering excellent mechanical strength and chemical resistance at high temperatures. PEEK screws offer a high strength alternative to PTFE fluoropolymers. Also this type of screws are used, because the are one of the few plastics compatible with ultra high vacuum. For this reason it is necessary to monitor the temperature of the sample holding plate, because if there the temperature drops down it is very likely that inadequate insulation, contacts with the sample holder exist or that the temperature probe attached to the sample holding plate is broken or not connected correctly. Measurements without the sample plate also show a fast temperature dropping-increase-dropping behavior, but with temperatures in the range of $\approx -160 to -180 degrees C$, which rules out that the sample plate is the only reason. One possible reason could be that the oxygen free copper has some disortions and oxidized through the frequent cooling runs. For this case a new oxygen free copper plate will be built.

- Thermal connections with the sample holder: The oxygen free copper clips do not conduct the temperature good enough via screwing them on the sample holder due to a low surface contact area.

- Shrinking of the parts in the cryostat due to the rapid decrease in temperature. After 100 minutes the equilibrium occurs.

4 Experimental Methods

4.1 Sample preparation

It has to be emphasized that preparing aqueous samples for cryogenic imaging is a task that requires great know-how and experience e.g. sample vitrification in amorphous ice using high pressure freezing etc. In this project only dry samples are prepared on coverslips using the protocol below. To have reproducible experiments every sample has to be prepared in the same way, for this reason a protocol for sample preparation has been done.

We used normal round glass coverslips of 12 mm diameter. Glass slides where first washed with Ethanol, followed by a drying with Argon gas step to eliminate any organic residue and dust particles, and then plasma cleaned for 15 minutes. After plasma cleaning, special care has to be taken not to touch the surface. Two different dyes were used: AF-647 and Atto-647N. For the AF-647 measurements, AF-647-streptavidin was used, diluted up to a concentration of 2 nM in a 200 nM unlabelled streptavidin solution, to avoid clusterization. For the Atto-647N measurements, Atto647-NHS ester was diluted from stock in PBS (phosphate buffer saline) to achieve a 2 nmol solution. 8 μl were incubated onto a central area of the coverslip and let it dry for a couple of minutes. Afterwards the coverslip is transferred to the sample holder, which is loaded in the cryostat. For room temperature measurements, after the sample is loaded in the cryostat, vacuum till $\approx 10^{-4} hPa$ is generated. All measurements at RT were done at $\approx 10^{-4} hPa$. For Cryogenic temperatures, the same procedure of sample preparation was followed, since we measured only dry samples at this stage. The samples were loaded into a warm cryostat which was then cooled down. After loading of the sample, the cryostat is closed and vacuum is generated. After several minutes a vacuum of $\approx 10^{-}5$ hPa is reached, which turned out to be the ideal point to fill the cryostat with liquid nitrogen. As soon as the working range temperatue of $\approx -160 to - 180 degrees C$ is reached (after $\approx 60 mins$) the valves of the vacuum pump are closed and the pump is stopped. Due to the fact that the vibrations of the vacuum pump disturb the process of measuring, it is recommended to wait until the rotation-frequency is near to zero.

4.2 Photostability measurements

Alexa-647 and Atto-647 have been tested for photostability measurements at room temperature and at cryogenic temperatures. All of the measurements were accomplished at the same conditions, to generate reproducible data:

- The Laser power on Laser I was chosen to have the same intensity as Laser II ($180 W/cm^2$).

- The exposure time of both lasers were 100ms with alternated polarized imaging mode.
- The imaging interval was 100ms.
- 1400 frames were done for room temperature measurements and 1800 frames were done at cryogenic temperatures, due to the fast bleaching of the dyes at room temperatures.

4.3 Analysis

Single molecules were detected and localized by using a Maximum Likelihood Estimator implemented in the ThunderSTORM ImageJ plugin [30]. Independently of tracking, the position of the molecules was averaged during the imaging period by using the localization merging algorithm implemented in ThunderSTORM. For plotting the normalized cumulative sum of detections, a vector containing the number of detections for all molecules analyzed was first sorted in ascending order and the cumulative sum of detections was calculated. The new vector was finally normalized by division with the overall number of detections and multiplication with the average number of detections for a particular molecule [31]. The data analysis part is assisted by Dipl.Ing. Magdalena Schneider.

5 Results and Discussion

5.1 Measurements at room temperature (T=293K)

AF-647 molecules measured at RT showed a relatively fast photobleaching (Figure 28 and Figure 29).We see a decrease of the active molecules after several hundreds of frames. This can be seen even by eye in the super resolution movies: in the first frames, we see several tens of active molecules per frame, which almost disappeared after 300 s. To quantify the photostability, we counted the number of localizations per frame. The detections over time (Figure 29) show an exponential decrease of localizations. All measurements were done at an existing vacuum $< 10^{-4} hPa$. Due to the absence of oxygen, it is expected that the photobleaching is reduced even at room temperatures.

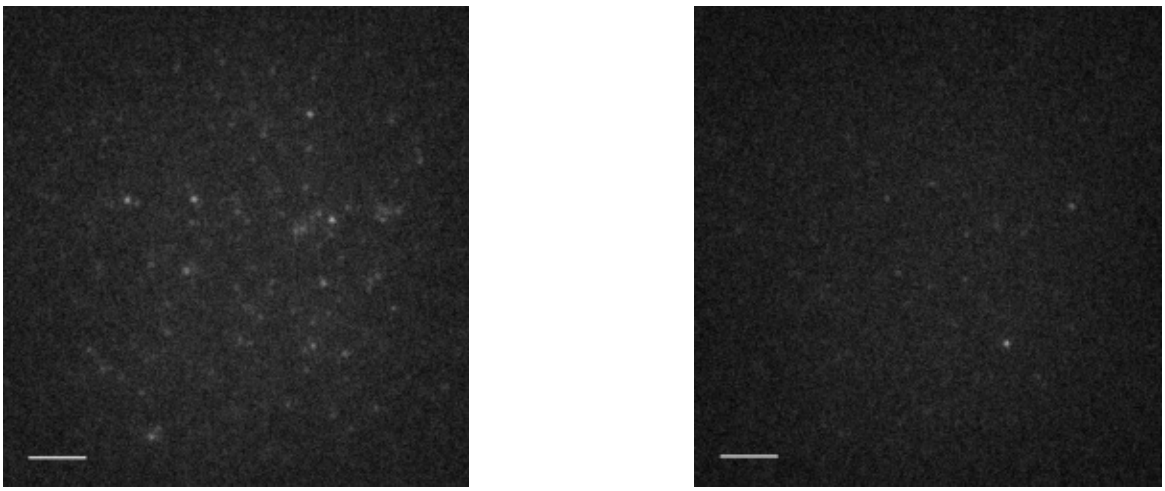

(a) AF-647 at t=0s

(b) AF-647 at t=300s

Figure 28: Comparison at t=0s and t=300s of AF-647 at RT. Even within the short timespan of 300 seconds photobleaching is clearly visible by eye.(Scale bar: 10 μm)

Due to the well known fact that oxygen is a strong triplet quencher, the removal of oxygen results in an extended life-time of the dark state. According to an extended life-time of the dark state the off-times increase, which may cause also a slowing down of the photo-bleaching.

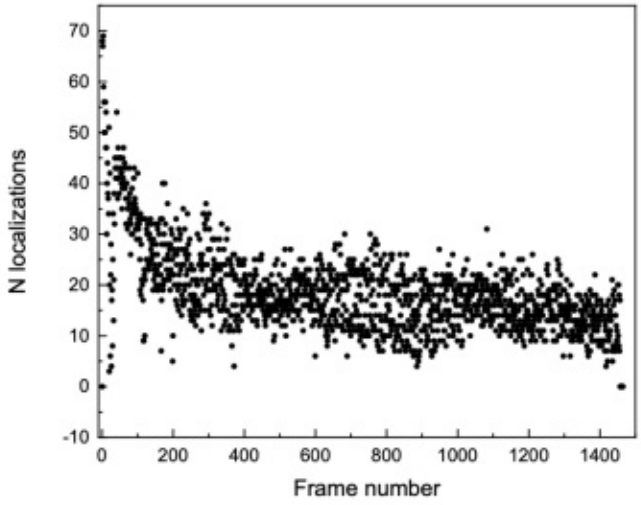

Figure 29: Detections over time of AF-647 at room temperatures.

Looking at the brightness of the molecules, we see in figure 30 the recorded photons obtained per molecule in a frame (a) . If we merge the frames (b) we see that the number of photons increases an order of magnitude. This photon numbers lead to a localization precision of $\approx 5nm$(figure 31).

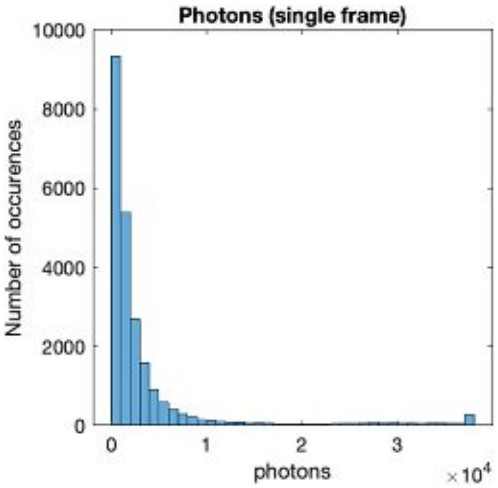

(a) Photons per molecule of AF-647 at room temperature.

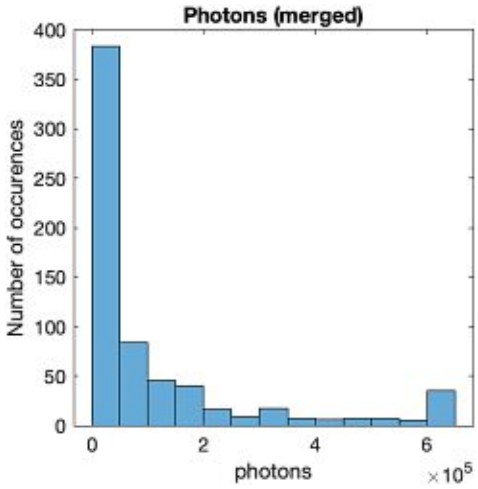

(b) Photons per molecule with clustered frames of AF-647 at room temperature.

Figure 30: AF-647. To quantify the photon yield the total number of detected photons was evaluated of a single frame and a merged frame.

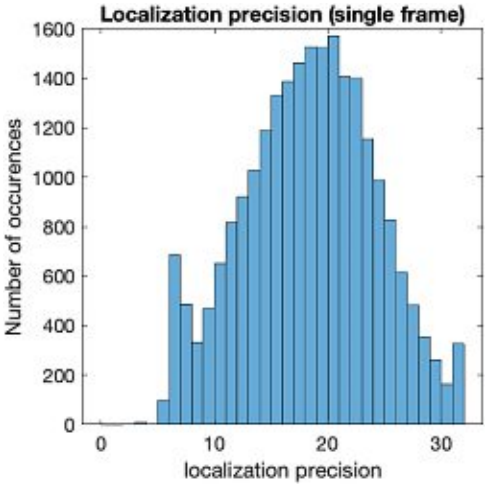

(a) Localization of AF-647 at room temperature.

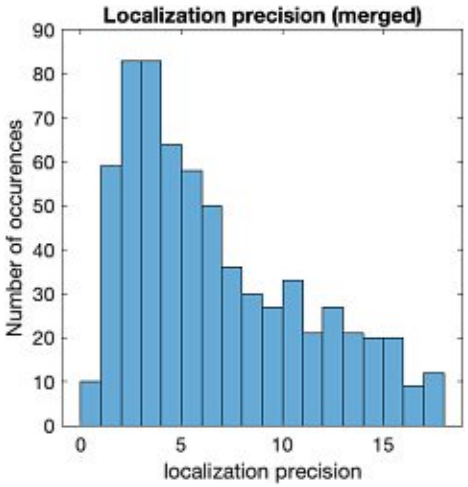

(b) Localization precision with merged frames of AF-647 at room temperature.

Figure 31: AF-647. The localization precision calculated of a single frame and merged.

For comparison reasons Atto647N dissolved in PBS dyes were also measured under the exact same conditions. It is clearly visible that the whole spot of the dye, which has been chosen to do the measurement has completely bleached after 300 seconds(Figure 32). We see a decrease of the active molecules after several hundreds of frames. This can be seen again by eye in the super resolution movies: in the first frames, we see around 15 molecules per frame, which completely disappear after 300 s. The detections over time (Figure 33) show again an exponential decrease of localizations.

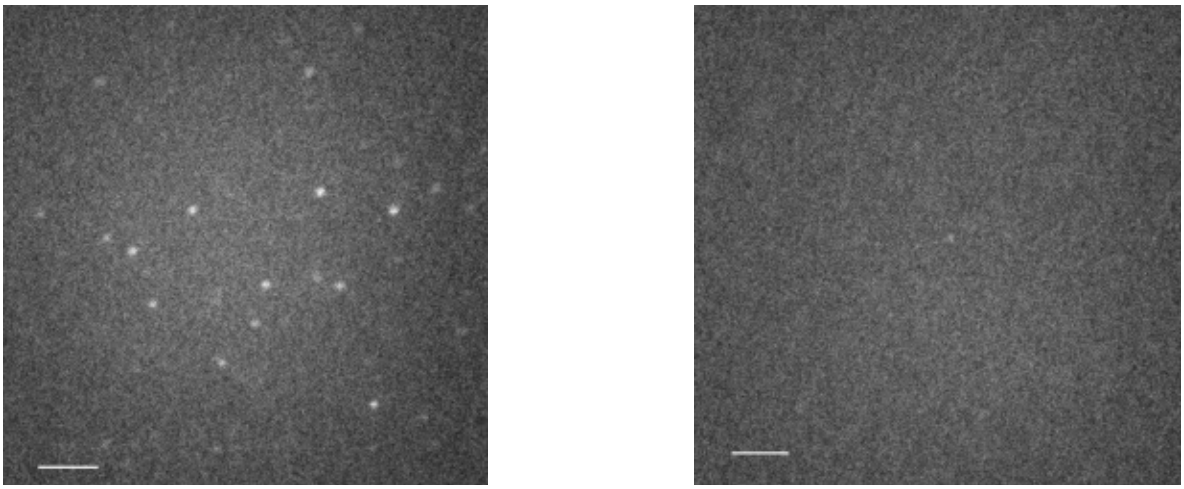

(a) Atto-647 at t=0s (b) Atto-647 at t=300s

Figure 32: Comparison at t=0s and t=300s of an Atto-647 dye. After 300 seconds of measurement time not a single molecule is visible by eye.(Scale bar: 10 μm)

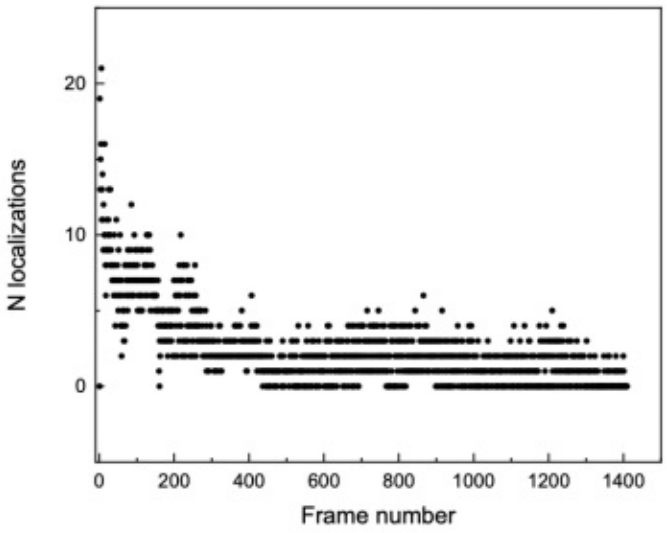

Figure 33: Detections over time of Atto-647 at room temperatures.

In figure 34 we see, the recorded photons per molecule per frame (a) for Atto-647 . If we merge the frames (b) we see that the number of photons increases an order of magnitude. This photon numbers lead to a localization precision of below $5nm$ (figure 35). We see that Atto-647N molecules photobleached at a faster rate than AF-647, however the molecules were much brighter. The number of collected photons were higher, which leads to better localization precisions.

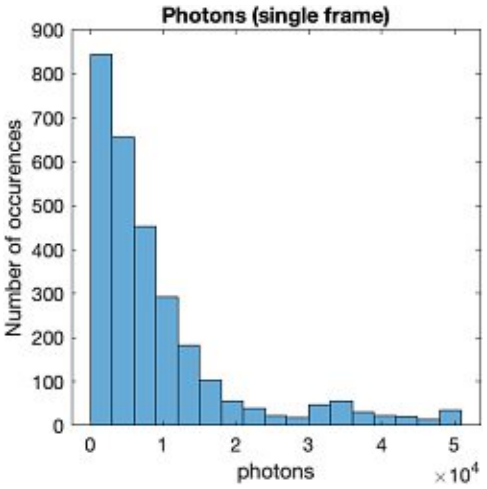

(a) Photons of a single frame of Atto-647 at room temperature.

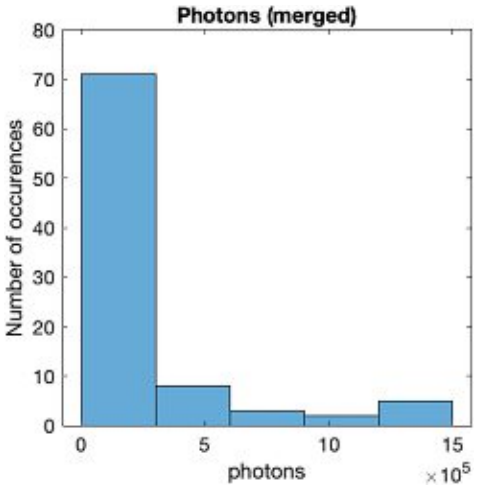

(b) Photons of a merged frame of Atto-647 at room temperature.

Figure 34: Atto-647. To quantify the photon yield the total number of detected photons was evaluated in a single frame and merged.

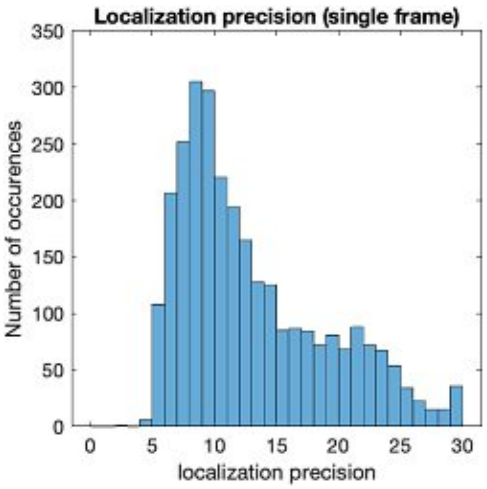

(a) Localization precision of a single frame of Atto-647 at room temperature.

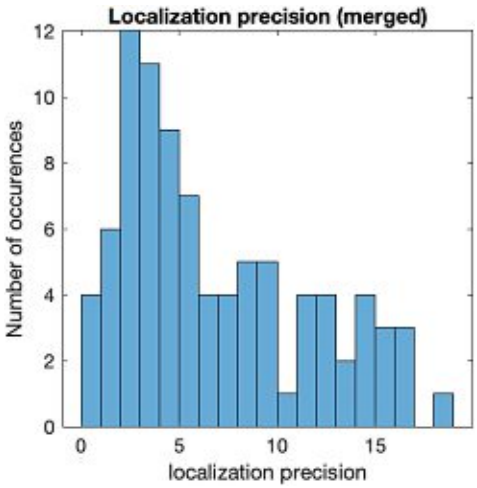

(b) Localization precision of a merged frame of Atto-647 at room temperature.

Figure 35: Atto-647. The localization precision calculated of a single frame and a merged frame.

5.2 Measurements at cryogenic temperatures (T=113K)

Due to the absence of oxygen and the low temperature, it is expected that the photobleaching is even more reduced at room temperatures. All measurements have been done at an existing vacuum of $\approx 10^{-6} hPa$ and a temperature of T=113K. AF-647 molecules measured at CT showed nearly no photobleaching (Figure 36 and Figure 37). We see a nearly constant value of the active molecules after several hundreds of frames. After 400 seconds in the super resolution movies no visible photobleaching can be seen by eye. The detections over time (Figure 37) show nearly no decrease of localizations. However, we also observe an increase in background fluorescence.

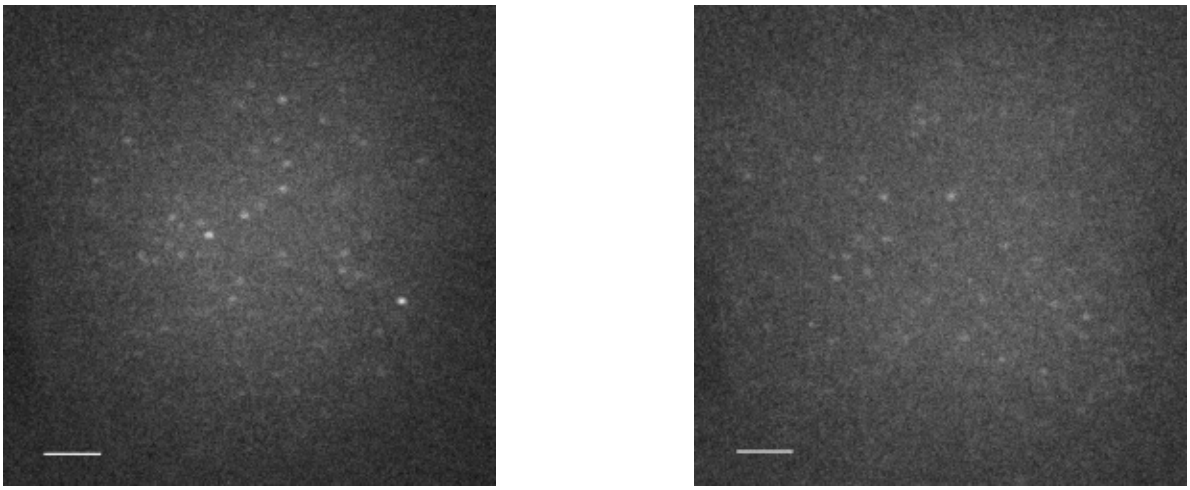

(a) AF-647 at t=0s

(b) AF-647 at t=400s

Figure 36: Comparison at t=0s and t=400s of AF-647. (Scale bar: 10 μm)

Photobleaching is strongly suppressed at cryogenic temperatures. There is barely any photobleaching visible within a time span of $\approx 400s$.

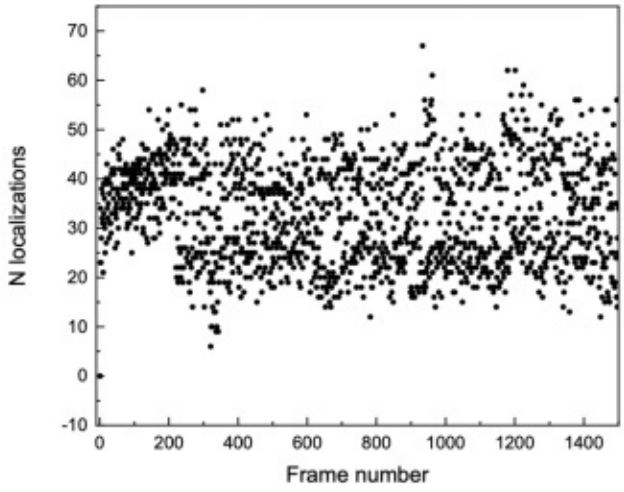

Figure 37: Detections over time of AF-647 at cryogenic temperatures.

Looking at the brightness of the molecules, we see in figure 38 the recorded photons per molecule (a) . If we merge the frames (b) we see that the number of photons per molecule increases an order of magnitude. At CT the localization precision of the merged frames increases to $< 5nm$ for AF-647(figure 39).

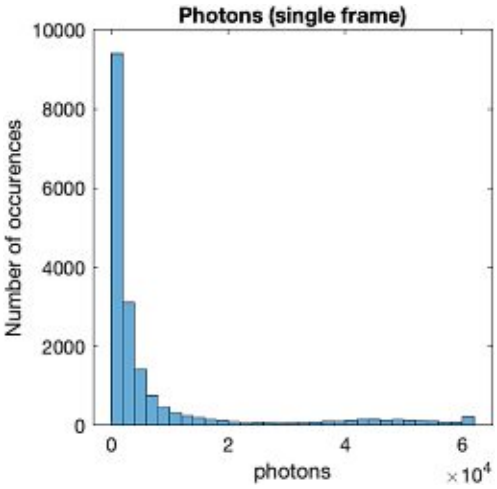

(a) Photons of a single frame of AF-647 at cryogenic temperature.

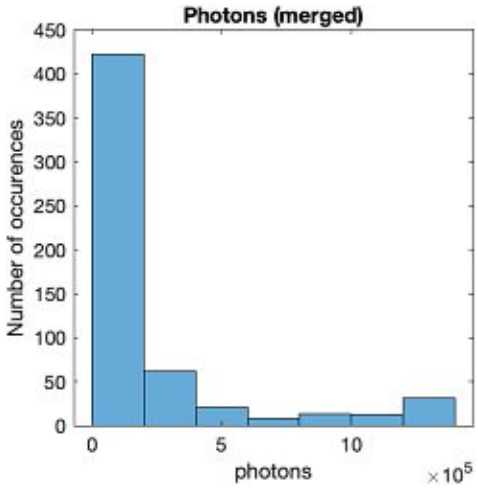

(b) Photons of a merged frame of AF-647 at cryogenic temperature.

Figure 38: AF-647. To quantify the photon yield the total number of detected photons per molecule was evaluated of a single frame and a merged frame.

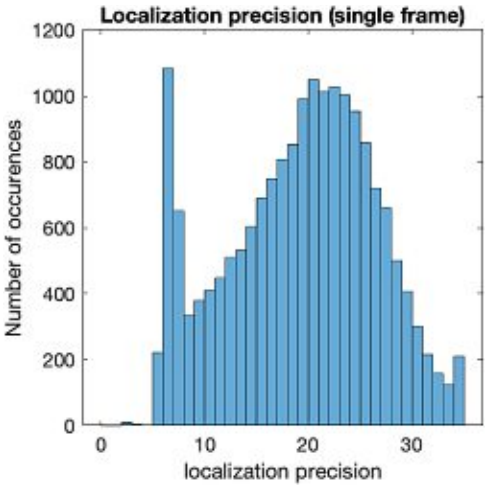

(a) Localization precision of a single frame of AF-647 at cryogenic temperatures.

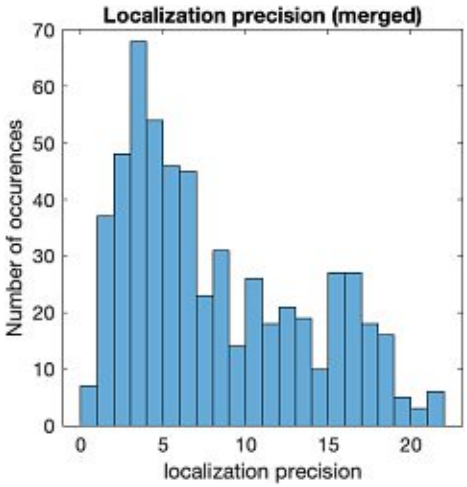

(b) Localization precision of a merged frame of AF-647 at cryogenic temperatures.

Figure 39: AF-647. The localization precision calculated of a single frame and a merged frame at cryogenic temperatures.

Despite the fact that experiments with a measurement time of < 1800 frames are related as short time measurements the collected number of photons clearly increased. The results for Atto-647 look quite similar (figure 40 and figure 41) to those of AF-647, except a difference in the brightness. The number of photons collected from Atto-647 is higher than of AF-647, which makes Atto-647 easier to detect and a lot brighter in the camera. The higher number of collected photons for Atto-647 also leads to a better localization precision.

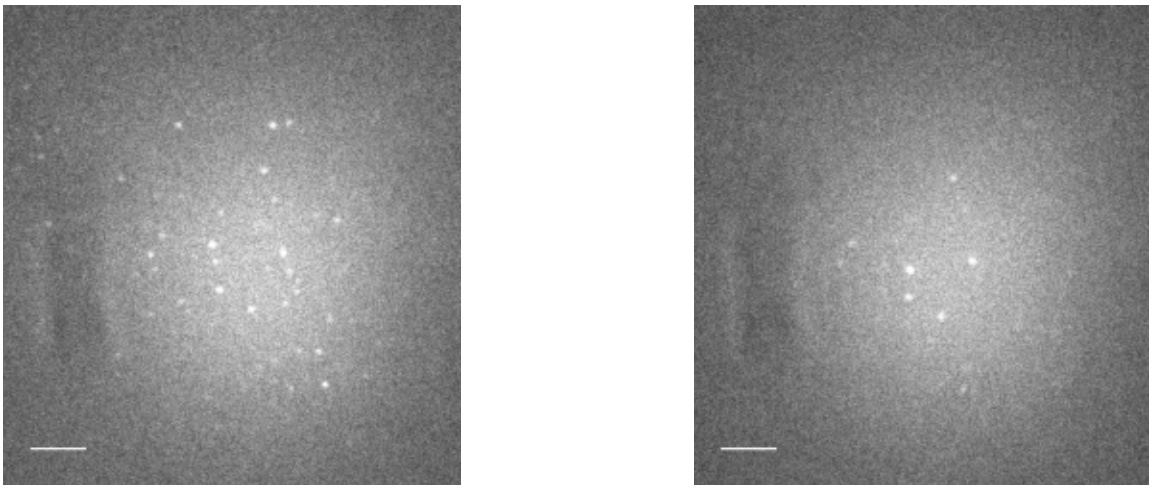

(a) Atto-647 at t=0s (b) Atto-647 at t=400s

Figure 40: Comparison at t=0s and t=400s of a single spot of an Atto-647 dye. (Scale bar: 10 μm)

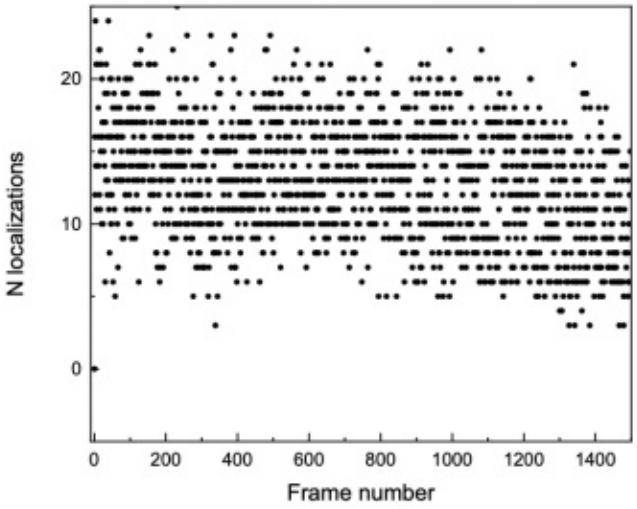

Figure 41: Detections over time of Atto-647 at cryogenic temperatures.

The number of detections over time also show a nearly constant value of localizations. Looking at the brightness of the molecules, we see in figure 42 the recorded photons obtained for a single frame (a) . If we merge the frames (b) we see that the number of photons per molecule increases an order of magnitude. This photon numbers lead to a localization precision of lower than $\approx 3nm$ (figure 43).

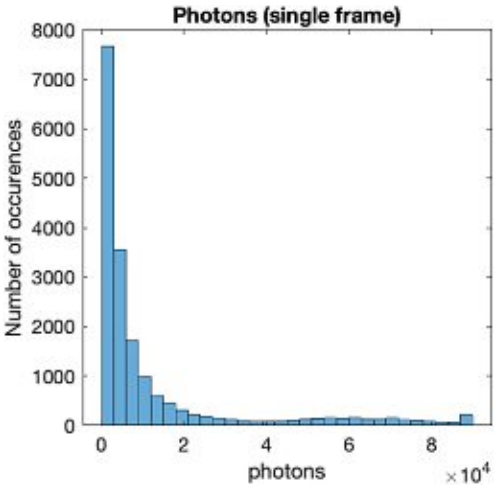

(a) Photons of a single frame of Atto-647 at cryogenic temperatures.

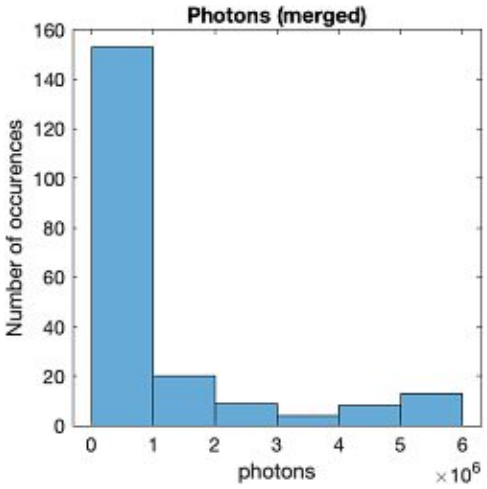

(b) Photons of a merged frame of Atto-647 at cryogenic temperature.

Figure 42: Atto-647. To quantify the photon yield the total number of detected photons per molecule was evaluated of a single frame and a merged frame.

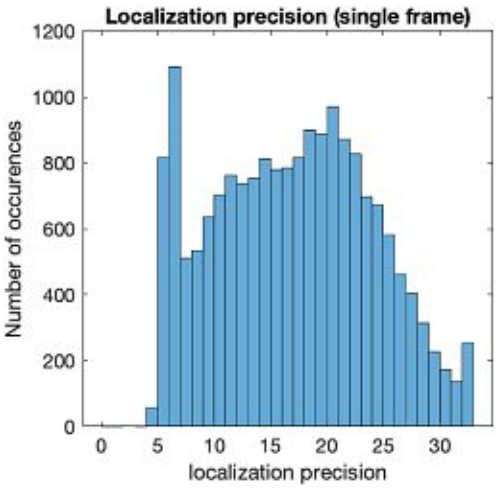

(a) Localization precision of a single frame of Atto-647 at cryogenic temperatures.

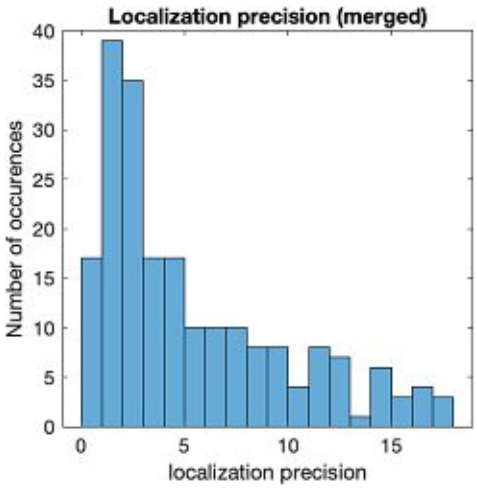

(b) Localization precision of a merged frame of Atto-647 at cryogenic temperatures.

Figure 43: Atto-647. The localization precision calculated of a single frame and a merged frame at cryogenic temperatures.

6 Comparison of RT vs CT

A direct comparison of AF-647 images at room temperature (≈ 20 degrees C) and at cryogenic temperature(≈ -150 degrees C) shows a much brighter appearance of the imaged molecule at CT after several hundreds of frames. It can be seen that the background at cryogenic measurements is enhanced.

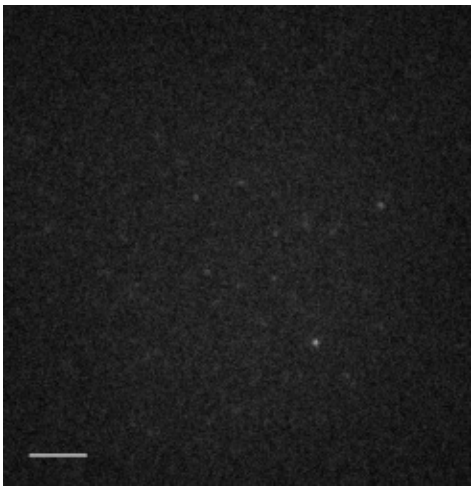

(a) AF-647 at RT after 280 seconds of measurement time.

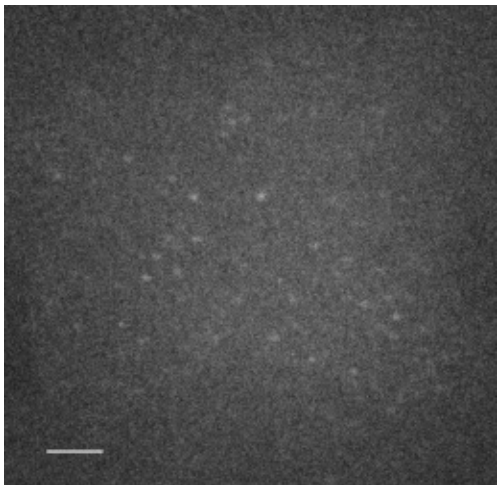

(b) AF-647 at CT after 400 seconds of measurement time.

Figure 44: Comparison of photobleaching at room temperature (≈ 20 degrees C) and cryogenic temperature(≈ -150 degrees C) of an AF-647 dye. (Scale bar: 10 μm)

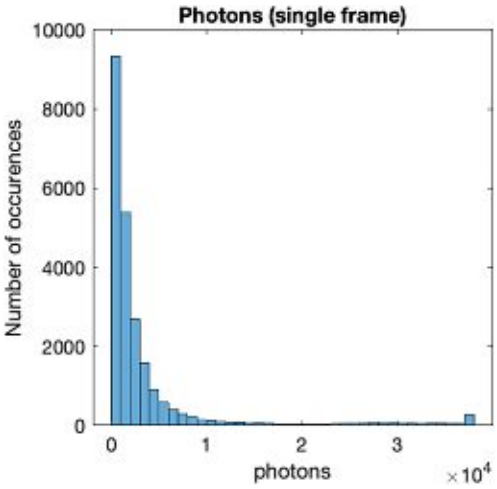

(a) AF-647 at RT

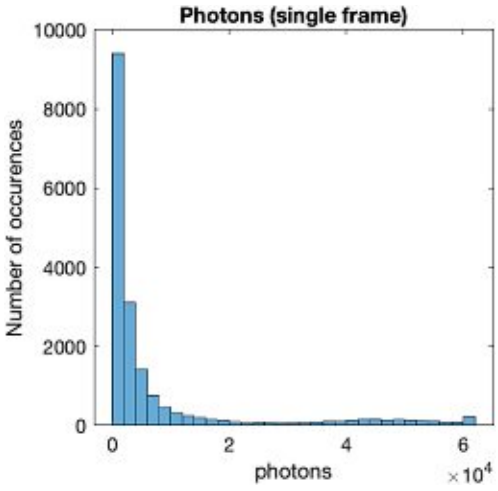

(b) AF-647 at CT

Figure 45: Comparison of the number of detected photons per molecule with (a) AF647 at room temperature and (b) at cryogenic temperature within a time span of 400 seconds.

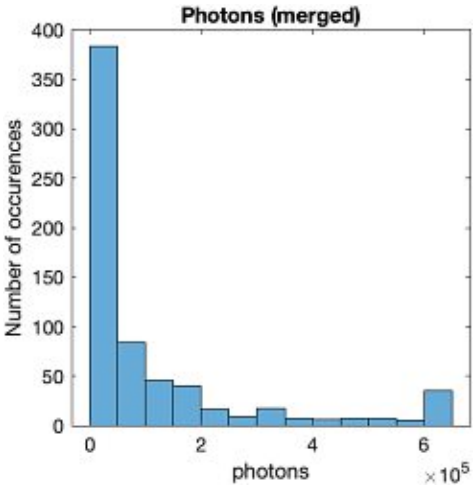

(a) AF-647 at RT

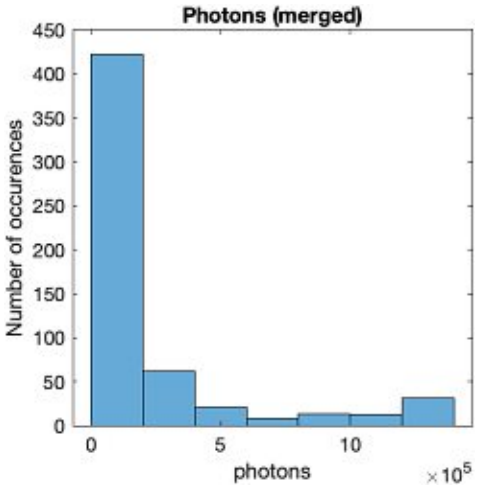

(b) AF-647 at CT

Figure 46: Comparison of the number of detected photons per molecule with clustered frames with (a) AF647 at room temperature and (b) at cryogenic temperature within a time span of 400 seconds.

The collected data of AF-647 at room temperature in vacuum(a) and at cryogenic temperature (b) within a time span of 400 seconds shows the difference in the photon yield. We see the maximum collected photons in a single frame to be around 3×10^4, while it doubles at cryogenic temperatures

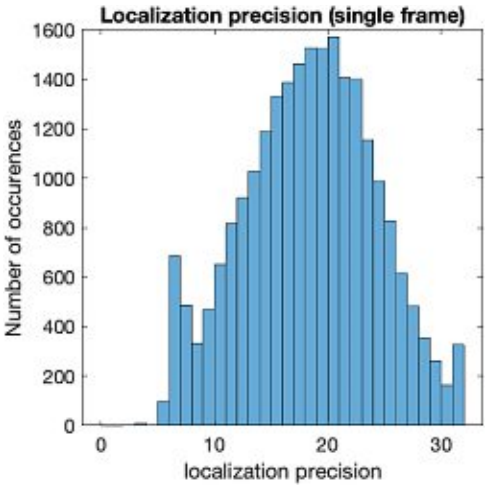

(a) Localization precision of a single frame of AF-647 at room temperatures.

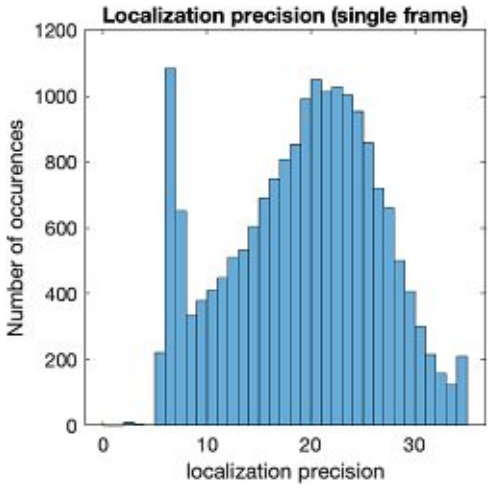

(b) Localization precision of a single frame of AF-647 at cryogenic temperatures.

Figure 47: AF-647. Comparison of the localization precision of a single frame with (a) AF647 at room temperature and (b) at cryogenic temperature within a time span of 400 seconds.

The localization precision of single frames did not improve at cryogenic temperatures, although there is a higher proportion of molecules localized with a precision of lower than $\approx 10nm$.

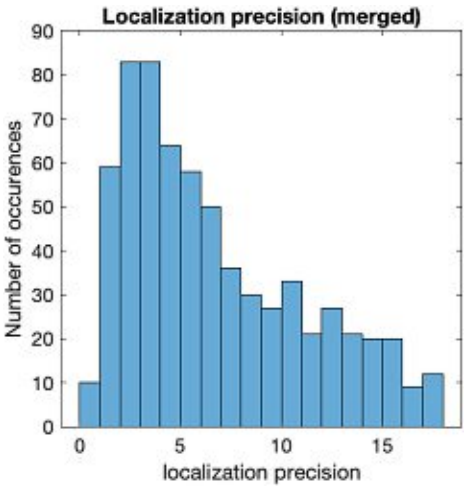

(a) Localization precision of a merged frame of AF-647 at room temperatures.

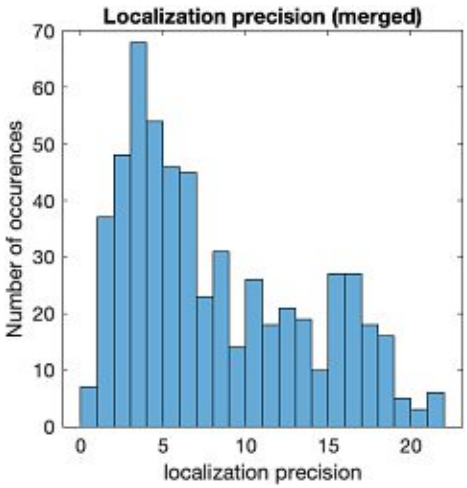

(b) Localization precision of a merged frame of AF-647 at room temperatures.

Figure 48: AF-647. Comparison of the localization precision of a merged frame with (a) AF647 at room temperature and (b) at cryogenic temperature within a time span of 400 seconds.

The same comparison images were taken for Atto-647. The brightness of Atto-647 molecules strongly increased switching to cryogenic temperatures. The signals are brighter to a high extend to make a sharp and focused image possible. The difference between cryogenic and room temperatures after a few hundred of frames is clearly visible.

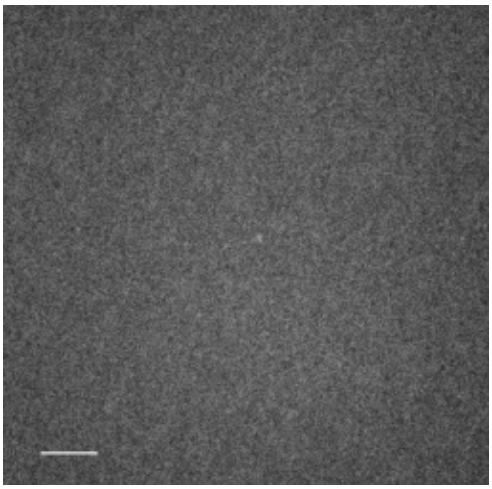

(a) Atto-647 at RT after 300 seconds of measurement time.

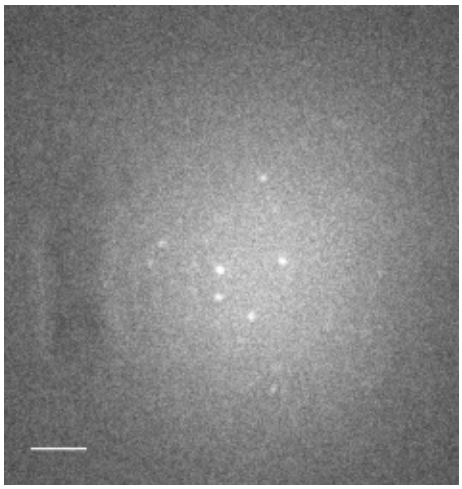

(b) Atto-647 at CT after 400 seconds of measurement time.

Figure 49: Comparison of room temperature ($\approx$ 20 degrees C) and cryogenic temperature($\approx$ -150 degrees C) of an Atto647 dye at t=400s. (Scale bar: 10 μm)

Analyzing the collected data of Atto-647 at room temperature (a) and at cryogenic temperature (b) within a time span of 400 seconds shows the difference in the photon yield. At room temperature the maximum numbers of collected photons of a single frame are $\approx 5 \times 10^4$, while at cryogenic temperatures the maximum number of collected photons of a single frame increases to $\approx 9 \times 10^4$. So the increase of detected photons of a single frame is around twice higher at cryogenic temperatures as at room temperatures under vacuum. Also higher increase in photons is detected for the number of photons in merged frames. At cryogenic temperatures the maximum number of detected photons with merged frames is more than 4 times higher than at room temperatures.

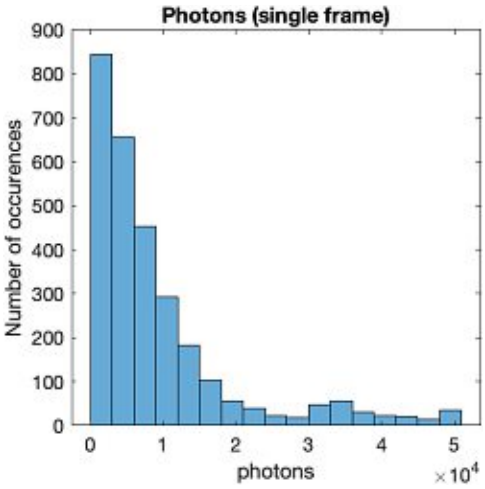

(a) Atto-647 at RT

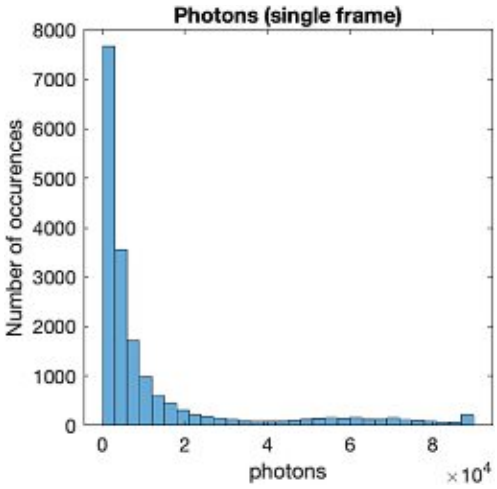

(b) Atto-647 at CT

Figure 50: Comparison of the number of detected photons of a single frame with (a) Atto-647 at room temperature and (b) at cryogenic temperature within a time span of 400 seconds.

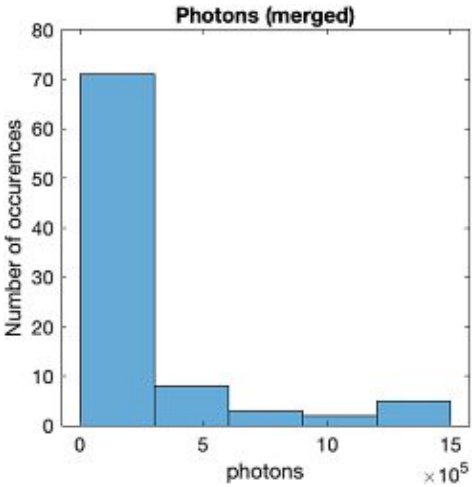

(a) Atto-647 at RT

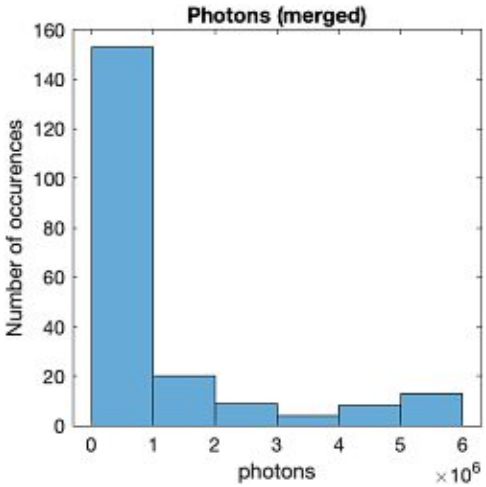

(b) Atto-647 at CT

Figure 51: Comparison of the number of detected photons of a merged frame with (a) Atto-647 at room temperature and (b) at cryogenic temperature within a time span of 400 seconds.

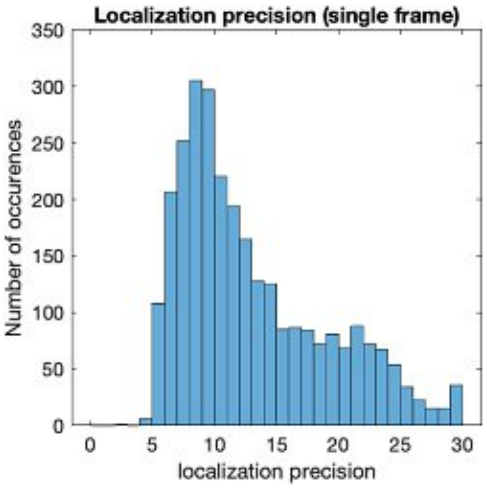

(a) Localization precision of a single frame of Atto-647 at room temperature.

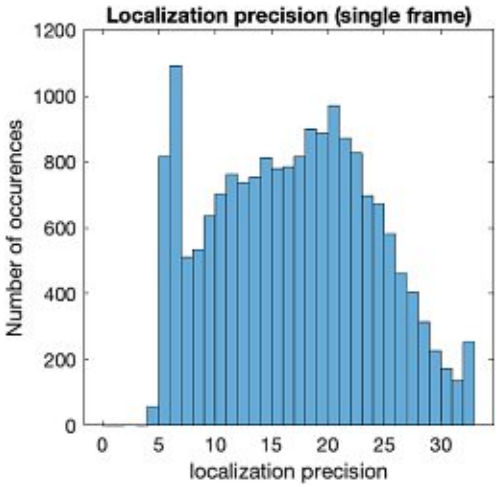

(b) Localization precision of a single frame of Atto-647 at cryogenic temperature.

Figure 52: Atto-647. Comparison of the localization precision of a single frame with (a) Atto-647 at room temperature and (b) at cryogenic temperature within a time span of 400 seconds.

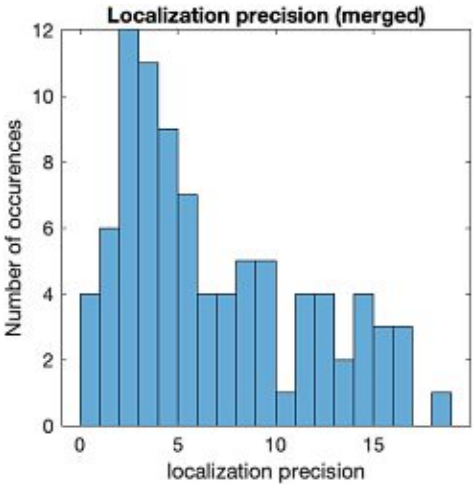

(a) Localization precision of a merged frame of Atto-647 at room temperature.

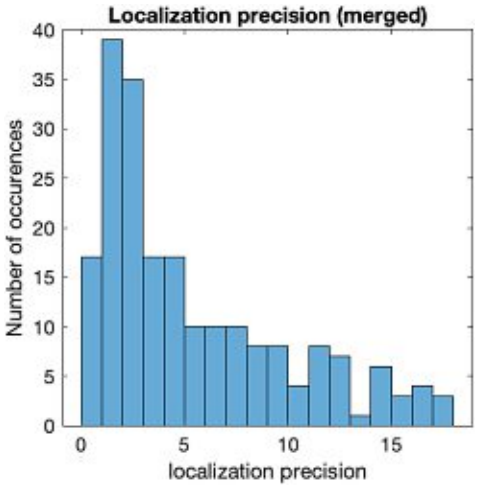

(b) Localization precision of a merged frame of Atto-647 at cryogenic temperature.

Figure 53: Atto-647. Comparison of the localization precision of a merged frame with (a) Atto-647 at room temperature and (b) at cryogenic temperature within a time span of 400 seconds.

The localization precision of a single frame at cryo temperatures is not improved in respect to the measurements at RT. This could be explained again by the increase of background fluorescence. However, due to the improved photostability, when we merge the frames, the signal to noise ratio increases and the localization precision is notably improved.

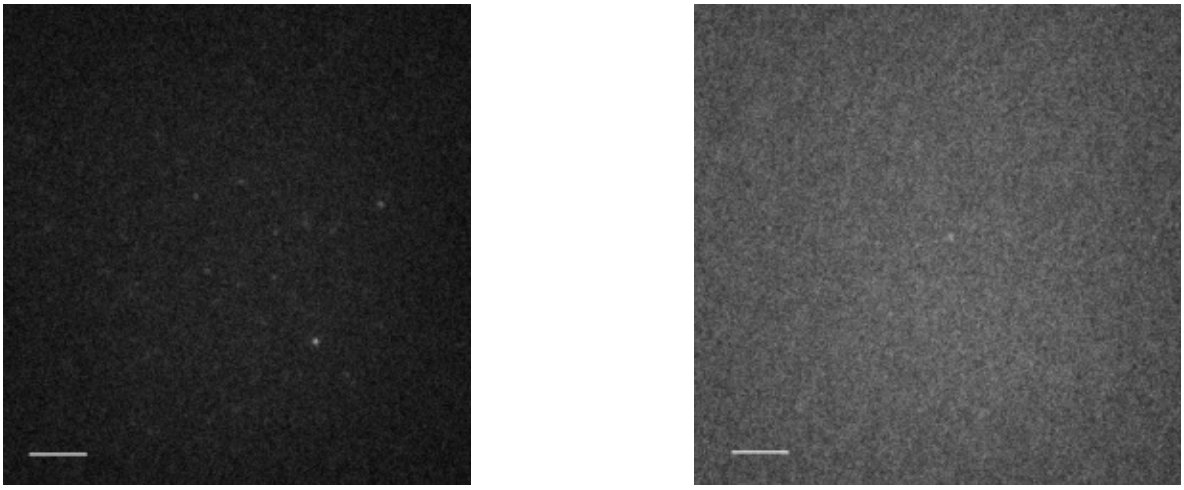

(a) AF-647 at RT (b) Atto-647 at RT

Figure 54: Comparison at room temperature of an AF647 and and Atto647 dye at t=300s. (Scale bar: 10 μm)

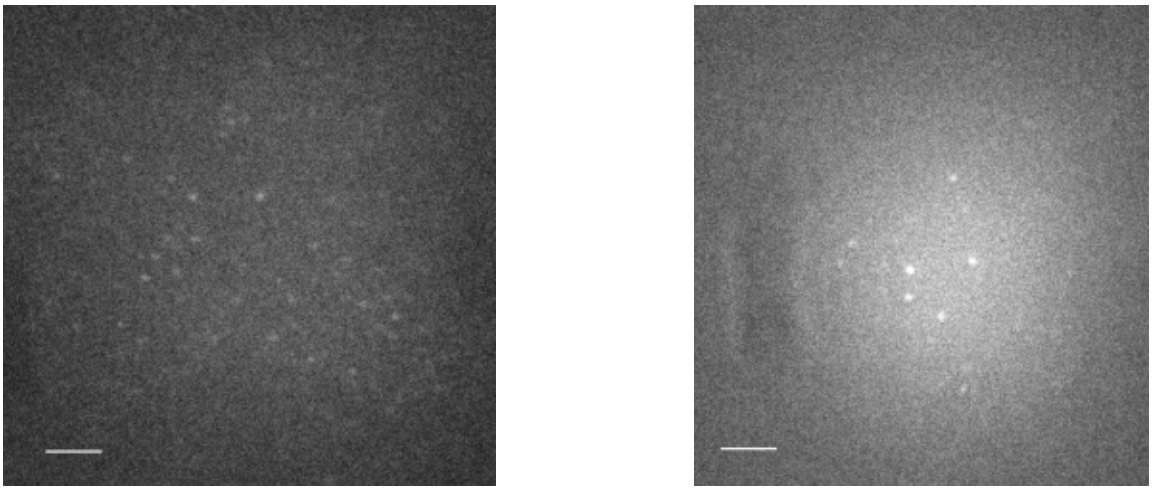

(a) AF-647 at CT (b) Atto-647 at CT

Figure 55: Comparison at cryogenic temperature of an AF647 and and Atto647 dye at t=400s. (Scale bar: 10 μm)

Also an increase in on/off-times were can be noticed. At cryogenic temperatures

the off times are greatly increased for AF-647, and in a lesser quality for Atto-647.

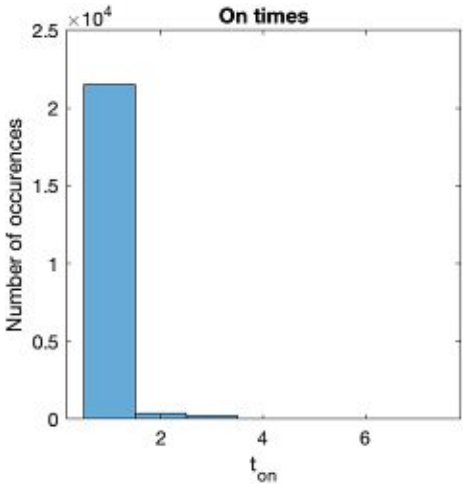

(a) On-times of AF-647 at RT.

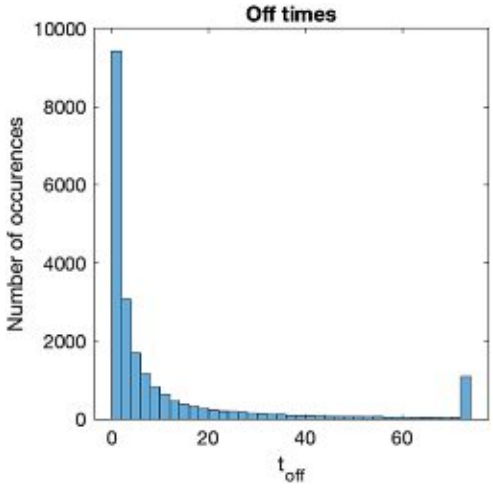

(b) Off-times of AF-647 at RT.

Figure 56: On and Off-times of AF-647 at room temperature within a measurement time of $\approx 400 seconds$.

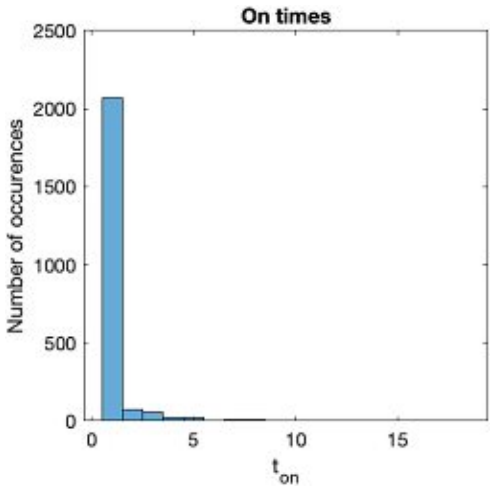

(a) On-times of Atto-647 at RT.

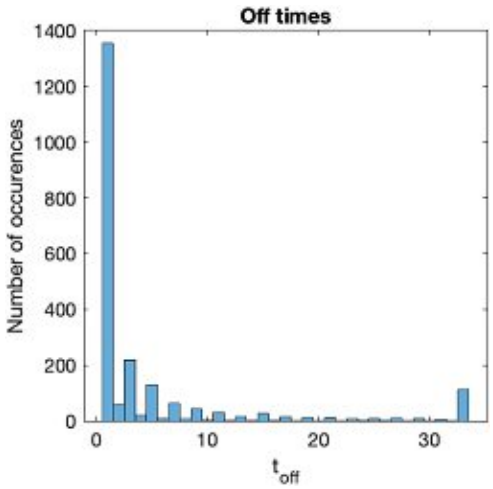

(b) Off-times of Atto-647 at RT

Figure 57: On and Off-times of Atto-647 at room temperature within a measurement time of $\approx 400 seconds$.

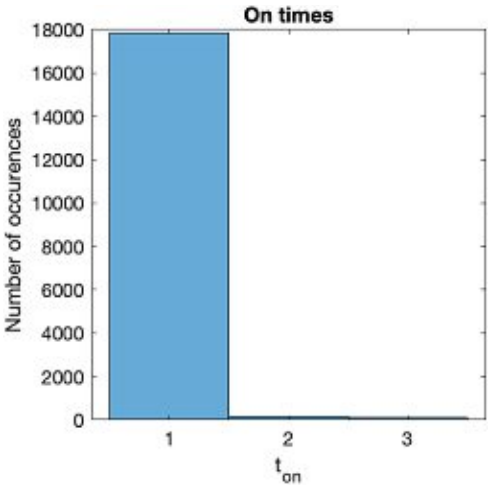

(a) On-times of AF-647 at CT.

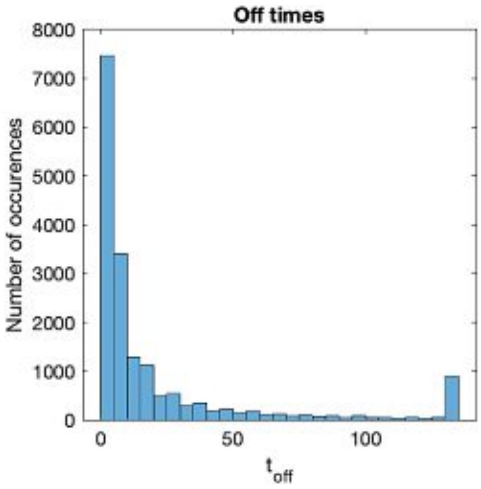

(b) Off-times of AF-647 at CT.

Figure 58: On and Off-times of AF-647 at cryogenic temperature within a measurement time of $\approx 400 seconds$.

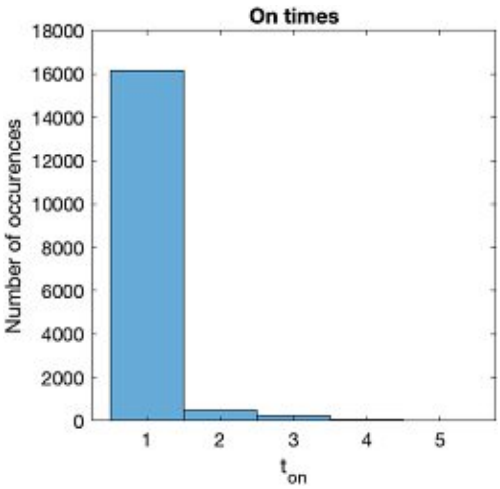

(a) On-times of Atto-647 at CT.

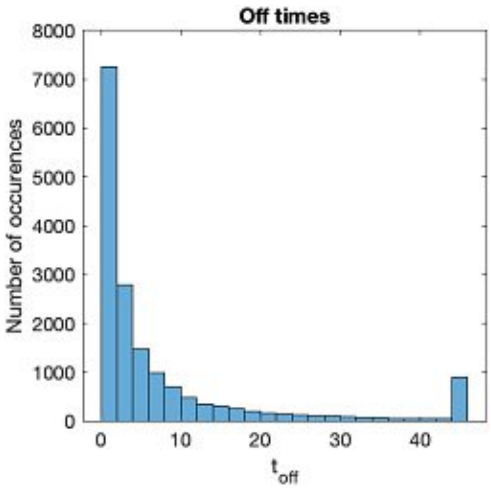

(b) Off-times of Atto-647 at CT

Figure 59: On and Off-times of Atto-647 at cryogenic temperature within a measurement time of $\approx 400 seconds$.

Higher off-times result in a lower on/off-ratio and supresses the blinking. In this case the possibility to seperate two molecules within one diffraction-limited spot increases.

7 Conclusion

This work's main focus was concerned as the development and testing of a new cryo-fluorescence microscopy system, which can be employed for single molecule microscopy at cryogenic temperatures. The system features excellent thermal and mechanical stability, is capable of single molecule imaging and is also applicable to long term measurements. The lowest temperatures reach $\approx 100K$ on the sample holder, but temperatures of $\approx 123K$ can be hold for several hours. Using this system, it is found that the photostability of organic dyes such as Atto-647, Alexa-647 can be improved when cooling down to $\approx 123K$. This results in an increase in localization precision. The resulting millions of detectable photons per molecule allow for single molecule localization with nanometer precision. Moreover, the blinking of Alexa647, Atto647 molecules is slowed down due to an increase of the off-times, which results in an higher on/off ratio. This provides the possibility to separate two molecules within one diffraction-limited spot temporally. For future experiments a vacuum insulated chamber can be applied to facilitate sample transfer of frozen dyes.

References

[1] [Online]. Available: https://www.jenabioscience.com/probes-epigenetics/reactive-components/reactive-fluorescent-dyes/maleimides/apc-009-af647-maleimide

[2] A. E., "Beitraege zur theorie des mikroskops und der mikroskopischen wahrnehmung." *Archiv fuer mikroskopische Anatomie.*, vol. 9, pp. 413–418, 1873.

[3] [Online]. Available: https://www.microscopyu.com/techniques/super-resolution/the-diffraction-barrier-in-optical-microscopy

[4] W. Ben, "Investigating ions' effects on the fluorescent protein dendra2," 08 2019.

[5] W. L. E. J. P. Dr., "Single molecule cryo-fluorescence microscopy," Ph.D. dissertation, Georg-August-University Goettingen, Göttingen, September 2016.

[6] C. Kirk and D. Tanya, "Future directions in advanced mycological microscopy," 10 2015.

[7] [Online]. Available: https://de.wikipedia.org/wiki/STED-Mikroskop#/media/Datei:STED_Mikroskop_PSFs.jpg

[8] H. Hannah, "Sharpening super-resolution by single molecule localization microscopy in front of a tuned mirror," Ph.D. dissertation, 01 2020.

[9] W. L. S. C. I. Gregor and J. Enderlein, "Ultra-stable and versatile widefield cryo-fluorescence microscope for single-molecule localization with sub-nanometer accuracy," *OPTICS EXPRESS 3770*, vol. 23, no. 3, 2015.

[10] [Online]. Available: https://www.sciencedirect.com/science/article/pii/S1367593114000623

[11] M. E. L. J. and R. R., "Cryogenic material properties database." *11th International Cryocooler Conference*, 2000.

[12] G. M. G. L., "Surpassing the lateral resolution limit by a factor of two using structured illumination microscopy," *J. Microsc.*, no. 198, pp. 82–87, (2000).

[13] H. S. W. . W. J., "Breaking the diffraction resolution limit by stimulated emission: stimulated-emission-depletion fluorescence microscopy." *Opt. Lett. 19*, pp. 780– 782, (1994).

[14] E. e. a. Betzig, "Imaging intracellular fluorescent proteins at nanometer resolution. science," no. 313, pp. 1642–1645, (2006).

[15] R. M. J. B. M. . Z. X., "Sub-diffraction-limit imaging by stochastic optical reconstruction microscopy (storm)," *Nat. Methods*, no. 3, pp. 793–796, (2006).

[16] W. D. B. TD, "Image artifacts in single molecule localization microscopy: why optimization of sample preparation protocols matters." *Sci Rep.*, January 2015.

[17] M. W. E. and K. L., "Optical detection and spectroscopy of single molecules in a solid," *Phys. Rev. Lett.*, vol. 62, pp. 2535–2538, May 1989.

[18] O. M. . B. J., "Single pentacene molecules detected by fluorescence excitation in a p-terphenyl crystal." *Phys. Rev. Lett.*, vol. 65, pp. 2716–2719, 1990.

[19] D. R. M. C. A. B. T. R. Y. . M. W. E., "On/off blinking and switching behaviour of single molecules of green fluorescent protein." *Nature*, vol. 388, pp. 355–358, 1997.

[20] C. C. . C. T., "Considerations on a laser-scanning-microscope with high resolution and depth of field." *Microsc. Acta.*, vol. 81, pp. 31–44, 1978.

[21] E. et al., "Imaging intracellular fluorescent proteins at nanometer resolution." *Science*, vol. 313, no. 1642-1645, 2006.

[22] R. M. B. M. Z. X, "Sub-diffraction-limit imaging by stochastic optical reconstruction microscopy (storm)," *Nat Methods*, vol. 3(10), no. 793-795, 2006.

[23] C. L. S. V. I. S. F. I. A. J. R. Mcintosh and D. Nicastro, "Cryo-fluorescence microscopy facilitates correlations between light and cryo-electron microscopy and reduces the rate of photobleaching," *J. Microsc*, vol. 227, no. 2, pp. 98–109, 2007.

[24] T. M. H. C. A. J. L. V. S. T. M. Jovin and S. Volker, "Three photoconvertible forms of green fluorescent protein identified by spectral hole-burning," *Nat. Struct. Biol*, vol. 6, no. 6, pp. 557–560, 1999.

[25] C. N. H. W. L. I. G. B. R. J. Enderlein, "Photon yield enhancement of red fluorophores at cryogenic temperatures," *ChemPhysChem*, vol. 19, pp. 1774–1780, 2018.

[26] R. K. C. Hagen and K. Grünewald, "Fluorescence cryo-microscopy: Current challenges and prospects," *Current Opinion in Chemical Biology*, vol. 20, no. 1, pp. 86–91, June 2014.

[27] M. W. T. A. J. K. S. J. F. G. A. Faas and T. H. Sharp, "Correlative cryo super-resolution light and electron microscopy on mammalian cells using fluorescent proteins," *Sci.Rep.*, vol. 9, no. 1, pp. 1–11, December 2019.

[28] R. et al., "Aberration-corrected cryoimmersion light microscopy," *Proc. Natl. Acad. Sci. U. S. A.*, vol. 115, no. 6, pp. 1204–1209, February 2018.

[29] [Online]. Available: http://www.ioffe.ru/SVA/NSM/Semicond/InP/thermal.html

[30] M. P. ek J.Borkovec Z vindrych G.M. Hagen, "Thunderstorm: a comprehensive imagej plugin for palm and storm data analysis and super-resolution imaging," *Bioinformatics*, vol. 30, no. 16, pp. 2389–2390, 2014.

[31] P. R. R. B. S. M. et al., "Unscrambling fluorophore blinking for comprehensive cluster detection via photoactivated localization microscopy." *Nat Commun*, vol. 11, no. 4993, 2020.